First evidence of a lake at Ancient Phaistos (Messara Plain, South-Central Crete, Greece): Reconstructing paleoenvironments and differentiating the roles of human land-use and paleoclimate from Minoan to Roman times

Matthieu Ghilardi,[1] David Psomiadis,[1,2] Valérie Andrieu-Ponel,[3] Maxime Colleu,[1,4] Pavlos Sotiropoulos,[5] Fausto Longo,[6] Amedeo Rossi,[6] Vincenzo Amato,[7] Françoise Gasse,[1] Laetitia Sinibaldi,[1] Mélanie Renard,[3] Andrew Bicket,[8] Doriane Delanghe,[1] François Demory[1] and Jules Fleury[1]

Abstract

Phaistos was one of the most important Minoan palaces in Crete and previous studies have addressed its relationship with the paleo-seashore position during historical times. Here, we reconstruct the environmental evolution of Phaistos from Early Minoan to Roman times. Study of two stratigraphic sections and nine boreholes drilled in the westernmost part of the Messara Plain has revealed the stratigraphy of the Mid- to Late-Holocene sediments. Laboratory analyses comprise granulometry, magnetic susceptibility measurements and identification of mollusks, diatoms and pollen grains. Eighteen radiocarbon dates provide a robust chronostratigraphy. In addition, a geophysical survey (electric resistivity tomography (ERT) method) was conducted to reveal the sub-surface morphology in the coring area. The results reveal that a freshwater lake existed from ca. 2100–2000 BC to ca. 1200–1100 BC, which subsequently became swampland until ca. 700 BC. A lake retreat is identified at ca. 1200–1000 BC and can be interpreted as resulting from the 3.2 cal kyr BP rapid climate change (RCC) dry event, observed elsewhere in the Eastern Mediterranean. Subsequently, from the 7th to the 5th century BC, there was the input of detrital material and fluvial dynamics prevailed until at least Roman times. The origin of the lake and its disappearance are discussed in the context of regional climate change and local tectonic activity, without excluding possible human influences. We also reconstruct the vegetation history for the period from the Late Minoan to the Early Archaic period. Pollen analysis reveals a Mediterranean maquis landscape dominated by *Olea*, together with hygrophilous vegetation, and highlights a clear transition from limnic to swampy environmental conditions around 1100 BC. The pollen sequence is also important for assessing the impact of the 3.2 cal. kyr BP RCC event and for assessing the possibility of an abrupt discontinuity in human activity around Phaistos after the demise of the Minoan Civilization.

Keywords

coring, Crete, diatoms, geophysics, Minoan civilization, paleoenvironments, Phaistos, pollen analyses, 3.2 cal. kyr BP

Received 10 November 2017; revised manuscript accepted 16 February 2018

[1]UM34 AMU, CNRS UMR7330, IRD, Collège de France, INRA, Centre Européen de Recherche et d'Enseignement des Géosciences de l'Environnement (CEREGE), France
[2]Imprint Analytics, Technologiezentrum Mittelburgenland, Austria
[3]Institut Méditerranéen de Biologie et d'Ecologie marine et continentale (IMBE), AMU, CNRS UMR 7263, IRD 237, Université d'Avignon, France
[4]Université Paris-Sorbonne, France
[5]Terra Marine, Greece
[6]Dipartimento di Scienze del Patrimonio Culturale (DISPAC), University of Salerno, Italy
[7]Dipartimento di Scienze e Tecnologie per l'Ambiente ed il Territorio, Università del Molise, Italy
[8]Wessex Archaeology, UK

Corresponding author:
Matthieu Ghilardi, UM34 AMU, CNRS UMR7330, IRD, Collège de France, INRA, Centre Européen de Recherche et d'Enseignement des Géosciences de l'Environnement (CEREGE), Europôle de l'Arbois BP 80, 13545 Aix-en-Provence, Cedex 04, France.
Email: ghilardi@cerege.fr

Figure 1. Location map of the study area and of the drainage basin of the Geropotamos River (red line). Black dashed-line: drainage basin of rivers coming from the Ida mountain ranges. K: Knossos. Contour lines and elevations are from the SRTM data (Farr et al., 2007).

Introduction

The island of Crete, in the Eastern Mediterranean (Figure 1), is well known for hosting one of the most famous ancient civilizations, of the Minoans, who occupied the island from ca. 3000 to 1070 BC (Lefevre-Novaro et al., 2015; Marangou, 1992). The most prosperous cultural phase occurred from ca. 1900 BC until ca. 1450 BC (the proto- and neo-palatial periods), and as a reflection of the great political and economic power of the civilization, numerous palaces were built close to the sea, such as Knossos, Malia, Kato Zakros, Aghia Triada, Mochlos and Phaistos (Figure 1). Although the chronology and occupation history of the Minoan sites are relatively well documented (Watrous et al., 1993), the landscape configuration around palatial sites is unclear (Rackham and Moody, 1996) and few studies (Lespez et al., 2001, 2003; Roberts, 1979; Siart et al., 2010; Theodorakopoulou et al., 2009) have focused on the palaeogeographic reconstruction of the surrounding landscape. Until now, the Cretan landscape configuration during various archaeological periods was unclear, especially in Minoan times (Rackham and Moody, 1996). The Messara Plain, in south central Crete, hosts several major archaeological sites dating from Minoan times. Among them, Aghia Triada and Phaistos are the most famous palatial sites (La Rosa, 1992a, 1992b) that may have been established on a paleoshoreline during Early Minoan times, according to a geological hypothesis (Fytrolakis et al., 2005); however, archaeologists claim that during Minoan times, neither Phaistos nor Aghia Triada were coastal sites (Bintliff, 1977; La Rosa, 1992a, 1992b; Shaw and Shaw, 1995) and Kommos, or Matala, probably served as Phaistos' harbour (La Rosa, 1992b). This study aims to reconstruct the palaeoenvironmental context and landscape evolution around ancient Phaistos, former capital of the Minoan Kingdom, and specifically to determine whether its original location was on the shoreline of Tymbaki Gulf during Minoan times.

Geological, geomorphological and hydrological setting

The Messara Plain (ca. 362 km^2; Watrous et al., 1993) is an east–west oriented tectonic graben (Fassoulas, 2001). It is drained by the Geropotamos River and its tributaries (Figure 1; Fytrolakis et al., 2005). There is no permanent river or stream flow today. To the north, it is bounded by the Ida mountains (Mount Psiloritis, 2456 m a.s.l.; Figure 1) and to the south by the Asteroussia Hills (ca. 1230 m a.s.l.; Figure 1). To the west, near Ancient Phaistos, the narrow and incised Geropotamos River connects the Messara Plain to the Tymbaki coastal plain and the surrounding Tymbaki Gulf (Libyan Sea), where other Minoan sites, such as Kommos and Aghia Triada, are located (Figure 1). Several tributaries of the Geropotamos River mainly drain Ida Mountains, especially the Koutsoulidi and Mageros streams (Figure 1). To the east, the Geropotamos catchment (ca. 600 km^2) is separated from the Anapodaris catchment by a very smooth hilly range at 260 m above mean sea level (amsl) (Figure 1). The geological setting of the area is described in detail by Peterek and Schwarze (2002, 2004) and Fytrolakis et al. (2005). The geology comprises Cretaceous (to the south) and Jurassic (to the north) limestones, and locally Mesozoic dolomites, Jurassic schists and ophiolites. Terrestrial and marine deposits of Miocene–Pliocene age occur at the western end of the Messara Plain (marls, clays and sandstones; Figure 2). Flysch and Pleistocene continental deposits occur to the south. The Messara Plain consists of a thick accumulation of detrital material that formed during the Pleistocene and Holocene (Figure 2). Seismic and neotectonic activity is evident in the study area (Tsapanos, 2001), as well as land subsidence (Papadaki, 2014; Peterek and Schwarze, 2004). Multiple active fault lines intersect the plain as well as the shoreline on the west (Figure 2); among them the Aghia Triada, Vori and Mires active faults, responsible for vertical movements in the Late Pleistocene to Holocene (Peterek and Schwarze, 2004), occur around Phaistos (which is developed on a horst). Kelletat and Zimmermann (1991) pointed to a southward tilting of the area during historical times, with a subsidence of around 2–3 m by Minoan, and around 1.2 m by Roman times (Mourtzas and Marinos, 1994). This tectonic activity shaped the local landscape and resulted in significant changes during the Holocene. The Holocene evolution of the coastal plain of Tymbaki was studied in the mid-2000s via the drilling of deep boreholes near Phaistos–Aghia Triada (Fytrolakis et al., 2005; Figure 2). However, the

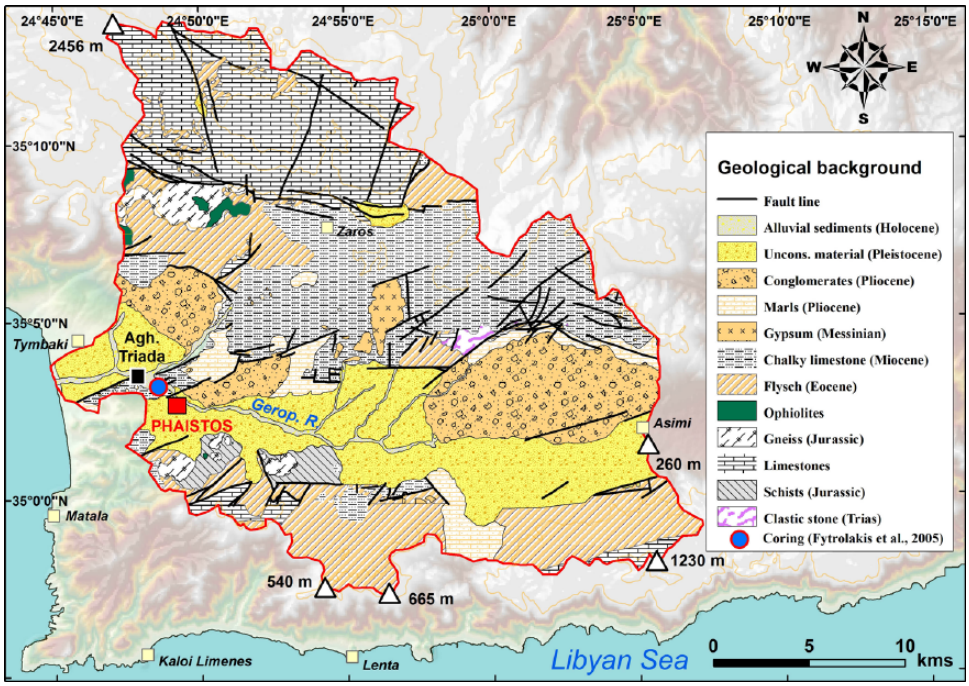

Figure 2. Geological map of the Geropotamos River. Data are from IGME maps (1: 50,000) and based on Peterek and Schwarze (2004) and Fytrolakis et al. (2005).

chronostratigraphy of the borehole drilled near Aghia Triada–Phaistos (Figure 2) remains unclear because of the lack of robust age control of the different facies that are not precisely identified. Mollusk assemblages are a promising chronological approach since a layer of marine shells has been identified at the depths of ca. 22–28 m below the surface (0/+6 m amsl), but it has not been radiocarbon dated. Despite the lack of age control, a possible marine incursion during Neolithic and Early Minoan Times was inferred by Fytrolakis et al. (2005). However, further coring is needed to elucidate the Mid- to Late Holocene chronostratigraphy in the surroundings of Phaistos.

Past climate and related alluvial evolution in Crete in the second half of the Holocene

The Aegean Sea is an important climatic transition area for the entire Eastern Mediterranean (Zervakis et al., 2004) and is particularly sensitive to climatic forcing, both at present (Roether et al., 1996; Theocharis et al., 1999; Zervakis et al., 2000) and in the past (Kuhnt et al., 2007; Marino et al., 2007). The Aegean Sea is distant and partially isolated from the North Atlantic oceanic circulation (Xoplaki, 2002). It is under the influence of multiple climate forcings, including the Siberian High (the extent of the polar vortex) and sub-tropical/tropical systems (Casford et al., 2003; Gogou et al., 2007; Macklin et al., 2010; Marino, 2008; Rohling et al., 2002). Although compared with the Last Glacial period, the amplitude of Mid- to Late-Holocene climate fluctuations was less pronounced, the eastern Mediterranean climate was less stable during this interval than previously thought (Kaniewski et al., 2013). For the last 5 kyr, climate reconstruction in South-Central and Eastern Crete is based mainly on past fluvial dynamics where phases of incision and aggradation, related to specific climatic conditions, were identified (Maas and Macklin, 2002; Macklin et al., 2010; Moody, 2000; Theodorakopoulou et al., 2009, 2012, 2017). In the nearby catchment of the Anapodaris River (East of Messara Plain; Figure 1), Macklin et al. (2010) recorded two major phases of coarse-grained aggradation dated to 4.86–4.2 and 3.4–3 cal. kyr BP; while in the Xeropotamos catchment (Eastern Crete), a phase of thick alluvial sediment accretion occurred from ca. 4.95 ± 0.3 cal. kyr BP (Theodorakopoulou and Bassiakos, 2017). Both pieces of work suggest that regional climatic cooling climate and episodes of heavy rainfall occurred from ca. 5.0 to 3.0 cal. kyr BP. The interval from 3.4 to 3.0 cal. kyr BP in Crete was especially humid (Macklin et al., 2010), and similar observations have been made throughout Mediterranean for the same period (Macklin et al., 2006; Zielhofer et al., 2008). Based on a study of Minoan flood deposits, Moody (2000) proposed a 'Minoan Little Ice Age' between 2000 and 1250 BC, possibly dominated by intense floods, and reinforcing the idea of a wet phase during the period from 5 to 3 cal. kyr BP. Moreover, the period following the so-called '4.2 ka event' (Zanchetta et al., 2016 and references therein) was characterized by mild conditions in Crete, with the onset of a rapid climate change (RCC) in the middle of the second millennium BC (Mayewski et al., 2004). This last period in the Aegean is attributed to the synchronous deflection or weakening of the major global monsoon and ocean-atmosphere circulation systems (Weiss, 2016). Focusing on the period of Minoan demise, Tsonis et al. (2010) determined that a strengthening of El Nino events began at about 1450 BC, making it highly probable that the area of Crete started to experience drier conditions from 1450 to 1200 BC. Although there are age discrepancies between proposed Holocene regional climate events, the study of Kaniewski et al. (2013) clearly identified that the Late Bronze Age crisis in Cyprus and Syria coincided with the onset of a 300-year drought cycle around 1200 cal. BC. Still in the Eastern Mediterranean, and at the same time, the fall of Mycenae is also ascribed to a climatic cause (Bryson et al., 1974; Carpenter, 1966; Weiss, 1982). Following the Late 2nd millennium BC climate aridification, Macklin et al. (2010) documented phases of incision and finegrained sediment accumulation in the Anapodaris catchment after 3 cal. kyr BP, which continued until ca. 2 cal. kyr BP, and suggested the occurrence of warmer and drier climatic conditions during the first millennium BC. Clearly, focused local investigations are needed to correlate small-scale climatic fluctuations and their possible impacts on human societies.

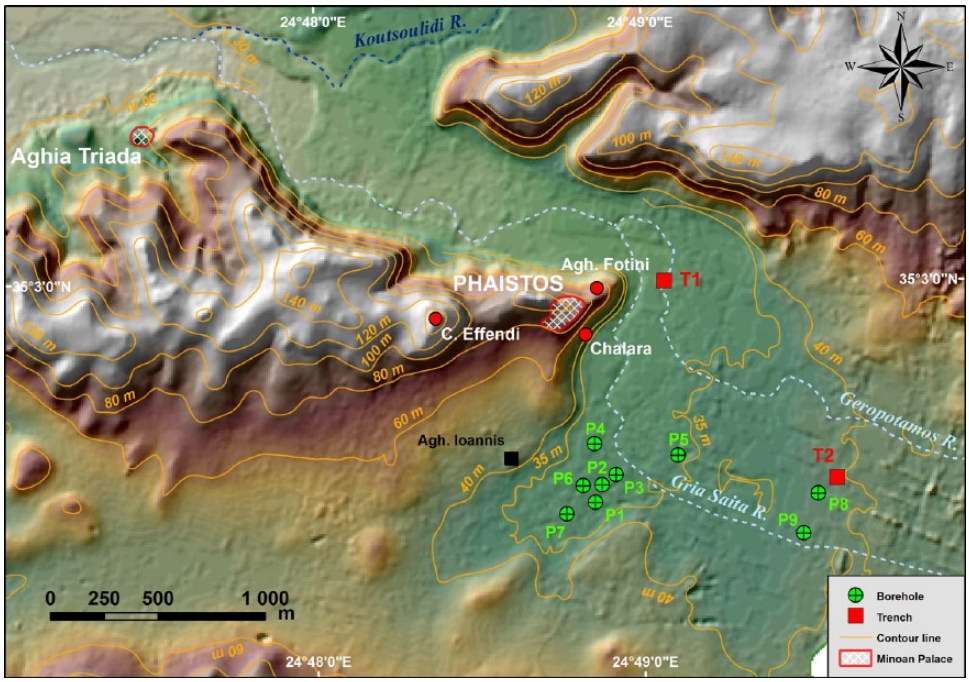

Figure 3. Locations of boreholes and trenches. The topographic data are derived from a photogrammetric analysis.

Human occupation of the western Messara Plain and the archaeological setting of Phaistos

Of the many settlements in Crete, Phaistos is one of the most important and long-lived. It is best known for the court-centred building – called a 'Palace' in the literature – erected at the beginning of the second millennium BC. Although the site had a longer occupation time, its vestiges are still largely unexplored. The earliest evidence of human occupation in the Phaistos area probably dates to the Late Neolithic period (4000–3500 BC; Di Tonto, 2009; Mentesana et al., 2016; Todaro and Di Tonto, 2008; Watrous et al., 2004). A recent re-examination of these earlier stages in the life of the site has revealed several phases of occupation from the Final Neolithic (Todaro, 2013), which continued until the first phase of Minoan civilization, better known as Pre-palatial (ca. 2700–2200 BC). The latter was a phase of major growth, especially of agriculture; at Aghia Triada, the processing of olives and grain are documented by grindstones and storage pithoi (Watrous et al., 2004).

A recent survey (Bredaki and Longo, 2009) has yielded new evidence suggesting that the 'urban' area of the Protopalatial Phaistos extended southward from the hilly range to the village of Aghios Ioannis and the hill of Christos Effendi to the west (see Figure 3 for locations). The archaeological evidence thus documents the existence of a vast settlement in this area, which was about as extensive as the later Hellenistic city (Bredaki and Longo, in press; Bredaki et al., 2012; Watrous et al., 2004).

In subsequent periods, the settlement contracted significantly, especially during the phases that followed the fall of the first palaces (ca. 1800–1450 BC), and again in the Mycenaean period (ca. 1450–1200 BC). This decline in size was probably related to the concomitant rise of the site of Aghia Triada, which from ca. 1600 to 1500 BC onwards was a powerful political centre with strong ties to the Neo-palatial and Post-palatial elites of Knossos (La Rosa, 1985, 2010). The settlement in the Phaistos area also appears to have shrunk significantly around 1220–1100 BC and during the Sub-Minoan, Proto-Geometric and Geometric periods (from ca. 1070 to 700 BC). At the time, it was very probably laid out in scattered housing groups, mostly on hilltops which facilitated control of the resources of the plain (Longo, 2015a, 2015b). Near the future city, Proto-Geometric and Geometric phases (10th to 8th centuries BC) have been recognized on the hill of Christos Effendi, on the Palace hill, and along the eastern slopes (Chalara; Figure 3). The area of Aghia Photini, on the northern slopes of the Palace hill (Figure 3) – once occupied by Pre-, Proto- and Neo-palatial buildings – yielded burials dating mainly to the Proto-Geometric and Geometric periods (Longo, 2015a, 2015b; Rocchetti, 1967–1968, 1969–1970).

The archaic and classical phases of Phaistos are still poorly documented, apart from the materials unearthed near the Palace and from the settlement of Chalara located downhill. The epigraphic documentation (collected in Bredaki et al., 2009; Marginesu, in press) and the numismatic evidence (Carbone, 2017, in press) bear witness, in any case, to the presence of a flourishing community. The city limits in the Hellenistic period can be deduced from the remains of perimeter walls – some already in plain sight, others excavated – northwest of Aghios Ioannis, on the hill of Christos Effendi, and at Chalara, and by the distribution of burial grounds (Longo 2015a, 2015b, in press; Rocchetti, 1967–1968, 1969–1970). After the destruction in about 150 BC (La Rosa, 1990) and a period of abandonment, the hills and the plateau were resettled (2nd to 4th centuries AD), as is confirmed by a survey (Bredaki and Longo, in press; Rossi, in press).

For the earliest historical phases, the issues of coastline configuration and distance from the sea remain unclear – although these factors are believed to have played a decisive role in the choice of the location for the settlement (as is also the case for other centres on the island, such as Malia).

Methods

Coring and trench sampling

Nine 50-mm-diameter vibracores were drilled in October 2011 and May 2014, in the lowlands of Ancient Phaistos, up to a maximum depth of 8.40 m below the surface (Table 1 and Figure 3). In addition, two stratigraphic sections (T1 and T2; Table 1 and

Table 1. Borehole and trench information.

Coring/trench reference	Latitude (WGS 84)	Longitude (WGS 84)	Absolute elevation (m)	Depth (m)
Phaistos 1 (P1)*	35°2′36.19″N	24°48′56.8″E	+34.9	2.25
Phaistos 2 (P2)*	35°2′38.61″N	24°48′58.05″E	+35.2	8.40
Phaistos 3 (P3)*	35°2′40.24″N	24°49′0.63″E	+35.1	7.35
Phaistos 4 (P4)*	35°2′44.79″N	24°48′56.71″E	+34.5	3.15
Phaistos 5 (P5)*	35°2′42.81″N	24°49′13.08″E	+35.2	4.20
Phaistos 6 (P6)*	35°2′38.46″N	24°48′54.82″E	+35.1	6.30
Phaistos 7 (P7)*	35°2′34.09″N	24°48′51.92″E	+34.9	6.30
Phaistos 8 (P8)†	35°2′37.55"N	24°49′37.52″E	+36.7	4.20
Phaistos 9 (P9)†	35°2′31.74"N	24°49′34.37″E	+37.2	6.30
T1	35°3′13.97″N	24°49′10.67″E	Top: +32.6/bottom: +29.4	–
T2	35°2′40.15"N	24°49′41.16"E	Top: +38/bottom: +32.80	–

*Borehole drilled in October 2011.
†Borehole drilled in May 2014.

Figure 3) were studied and sampled for laboratory analyses. Each borehole and both trenches were precisely levelled with Differential Global Positioning System Trimble R8 equipment.

Magnetic susceptibility measurements and grain-size analysis. Sediment cores P2, P5 and P7 were selected for the heterogeneity of their sediments and were sampled at 5 cm resolution, except for levels which included reworked material. Magnetic susceptibility measurements were made using an MFK1 magnetic susceptibility metre (Agico) at CEREGE (Aix en Provence, France), at frequencies of 976 Hz and 15616 Hz. The values were divided by the density of the dried samples to obtain mass-specific susceptibilities (χ). χ values reflect the contributions of diamagnetic, paramagnetic, ferromagnetic and imperfect antiferromagnetic particles (Dearing et al., 1996), but high values typically reflect the concentration of ferromagnetic particles.

The grain-size distribution of the fine fraction (<2 mm) was measured by laser diffraction granulometry at CEREGE. Samples were taken at 5 cm intervals. All samples were first heated to 450°C and mixed with a dispersing agent (0.3% sodium hexametaphosphate) to disaggregate the clay particles. For the calculation model, we used water as the medium (refractive index (RI) = 1.33 at 20°C), a RI in the range of that of kaolinite for the solid phase (RI = 1.56), and absorption coefficients of 0.15 for the 780 nm laser wavelength and 0.2 for the polarized wavelengths (Buurman et al., 1996, 1997).

Loss-on-ignition and carbonate ($CaCO_3$) content. Loss-on-ignition (LOI) measurements were made at CEREGE, following Dean (1974) and Bengtsson and Enell (1986). Sediment samples of approximately 1 g were taken at 10 cm intervals throughout the sequence. After drying at 105°C to constant weight, the samples were heated to 550°C for 7 h to estimate the organic content. A second heating phase, to 950°C for a further 7 h, was undertaken to assess the proportion of carbonate.

Diatom and pollen analyses. Diatom analyses were conducted on all cores but only core P2 (the interval from 6.80 and 6.50 m, five samples in total) contained enough material for analysis. Sediment (clay) of 0–5 g was treated using standard procedures (1:1 mixture of H_2O_2/water, 1:1 mixture of HCl/water), and repeated rinsing in distilled water (see Battarbee et al., 2001 for details). For each sample, at least 400 diatom valves were identified and counted using a light microscope (×1000 magnification). Specimens were identified following the species concept of Krammer and Lange-Bertalot (1986, 1988, 1991a, 1991b). However, many of the genera and species outlined therein have been re-assessed using the classification of Round et al. (1990) and synonyms are used here. Diatom concentrations were calculated using the dry weight of the sample.

Pollen analyses were conducted on cores P2, P3 and P6, which contained fine-grained material (stiff clays) that could potentially yield pollen; however, only core P2 had a sufficient pollen concentration and in which bioindicators were well preserved. Sampling was conducted every 5 cm for the depth interval from 8.30 to 5.25 m; only the interval from 7 to 5.80 m contained sufficient pollen grains for analysis. For the samples from this interval, at least 300 pollen grains, excluding aquatics, were counted. In total, 23 samples were analysed (samples at the depth of 6.85 m and 6.95 m were excluded because of poor preservation and scarcity of pollen grains). Chemical pre-treatment of the samples followed Nakagawa et al. (1998) and identifications were made ×500 magnification using the pollen reference collection of the IMBE Laboratory (Aix-en-Provence, France) and pollen photographic atlases (Beug, 2004; Reille, 1992, 1995, 1998). Charcoal microparticles (size >20 μm) were also counted.

AMS ^{14}C dating. The chronostratigraphy of the cores and trenches was established using a series of 18 AMS radiocarbon determinations from charcoal, organic matter, plant remains and peat samples (Table 2). The analyses were made in the Poznan (Poland) Radiocarbon Dating Laboratory. ^{14}C ages were calibrated using Calib Software Version 7.1 (Stuiver and Reimer, 1993) and the IntCal13 calibration curve (Reimer et al., 2013). In addition, a smoothing spline age-depth model (Figure 4) was constructed for core P2 (where the pollen analyses were conducted) for the interval from 8.40 to 5.80 m, using R software and the Clam package (Blaauw, 2010). Given the homogeneous texture of the sediments (fine clays), extrapolation of the depth age model for the interval from 6.55 to 5.80 m deep is regarded as reliable.

Electric resistivity tomography

The geometry and location of the main sub-surface structures were analysed using electric resistivity tomography (ERT). A computer-inversion programme (Res2Dinv; Loke, 2003) including the topography generates images of resistivity distribution along a cross-section below the survey line. ERT has been successfully used in various sub-surface field studies, especially in geomorphology (Beauvais et al., 2007; Ghilardi et al., 2017) and archaeology (Ghilardi et al., 2015; Quesnel et al., 2011; Siart et al., 2010). In this study, a 2D-resistivity tomography was obtained using the ABEM Lund Imaging System (Terrameter LS/4channel) with an array of 64 electrodes with a Schlumberger–Wenner reciprocal layout protocol. In the Messara Plain, data acquisition was conducted from 21 to 23 June 2013. ERT profiles

Table 2. Radiocarbon dating results.

Coring/trench reference	Depth (m)	Absolute depth above mean sea level (m)	Material	BP	Error ±	Cal. 2σ	Laboratory reference
P2	6.55	+28.62	Plant remains	2865	30	1122–930 BC	Poz-49261
P2	7.00	+28.17	Plant remains	2990	35	1378–1119 BC	Poz-49263
P2	7.20	+27.97	Plant remains	3110	50	1495–1264 BC	Poz-58147
P2	8	+27.17	Plant remains	3310	80	1772–1420 BC	Poz-58104
P2	8.40	+26.77	Plant remains	3550	50	2023–1750 BC	Poz-49264
P3	7.05	+28.02	Charcoal	3640	40	2136–1906 BC	Poz-49266
P5	2.67	+32.58	Charcoal	2180	30	366–166 BC	Poz-49268
P6	6.20	+28.85	Peat	2870	30	1130–931 BC	Poz-46522
P6	6.22	+28.83	Peat	2925	30	1257–1019 BC	Poz-46523
P7	5.20	+29.7	Charcoal	3630	35	2051–1895 BC	Poz-49270
P7	5.78	+29.12	Charcoal	4400	50	3328–2906 BC	Poz-49059
P9	4.8	+32.4	Charcoal	3130	50	1501–1271 BC	Poz-70961
P9	4.94	+32.3	Charcoal	2970	50	1381–1022 BC	Poz-70962
P9	5.47	+31.73	Charcoal	3070	35	1417–1257 BC	Poz-73607
T1	2.20	+30.40	Charcoal	117.13	0.42 pMC	Modern	Poz-52110
T1	2.56	+30.04	Charcoal	1120	30	AD 862–AD 994	Poz-52111
T1	2.90	+29.7	Charcoal	1730	30	AD 240–AD 391	Poz-52112
T2	4.2	+33.8	Organic sediment	2655	35	896–791 BC	Poz-56331

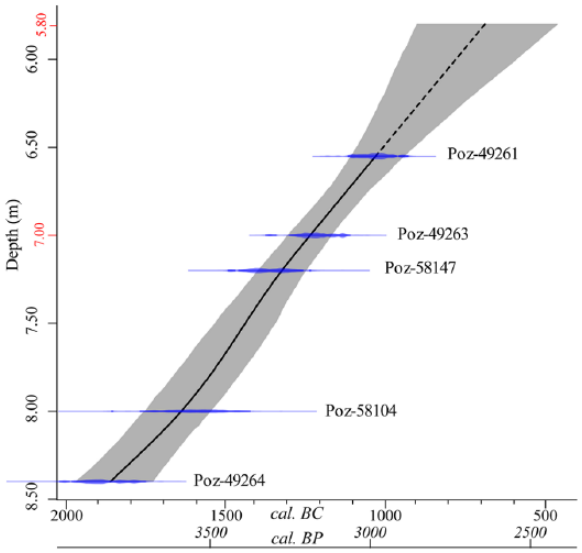

Figure 4. Age-depth model for core P2 (from 8.40 to 5.80 m depth) constructed using R software and the Clam package (Blaauw, 2010).

were conducted with an electrode distance of 2, 3, 4 and 8 m. The length of each of the five profiles ranged from 128 to 514 m (Figure 5). The ERT method, however, does not provide a unique interpretation, since different materials can have similar electrical properties. Consequently, the usefulness of the interpretation depends on a good knowledge of the local context and, preferably, should be validated with a geotechnical/coring investigation. It is common practice to correlate data derived from resistivity tomography (a non-destructive method) with the results of coring and sampling (Ghilardi et al., 2015, 2017).

Results

Borehole chronostratigraphy

Bedrock (chalky limestone) was only reached in core P1, at a depth of 2.25 m, below the modern swamp environment. For the other boreholes, based on bio-sedimentological analyses, six sedimentary units can be identified, described below.

Unit TR was only found in the westernmost part of the plain, in the lowermost part of core P7 (Figure 6, bottom right) and consists of reddish (lower part) to dark grey/reddish (upper part) silty clays with a mean grain-size generally from 10 to 40 μm. The total thickness is unknown and only 80 cm were collected in the sampler. Unit TR can be divided into two subunits. *Subunit TR1 (6.30–5.90 m)* consists of red clays. χ values are high, but they decrease towards the top of the subunit: from 150 (6.30 m) to 50 × 10^{-8} m^3/kg (5.90 m); χ_{fd}% values are constant and high, >10%, indicating a significant contribution from superparamagnetic particles. The carbonate content is <10%. The subunit is exclusively composed of terrigenous material (*Terra Rossa*). *Subunit TR2 (5.90–5.50* m). This subunit overlies TR1. It consists of a mixture of grey and red clays with relatively low χvalues (<50 × 10^{-8} m^3/kg) and with a carbonate content increasing from 10% (at the top of TR1) to ca. 45%. The transition from TR1 to TR2 is radiocarbon dated to 3328–2906 BC (Table 2). Thus, the age of the *Terra Rossa* deposits is from the late fourth Millennium BC.

Unit G was only found in the eastern part of the investigated area, in cores P8 and P9 (Figure 7). Due to the paucity of organic matter, no radiocarbon dating was done on these coarse layers. Unit G can be divided in two subunits based on the grain-size. *Subunit G1 (from 4.25–3.00 m depth in core P8 and from 6.30–6.00 m depth in core P9).* It consists of cemented (carbonate matrix), rounded pebbles (maximum size of 4 cm) and gravels, alternating with reddish (reflecting oxidation) medium- to coarse-grained sands. *Subunit G2* overlaying subunit G1, is composed of homogeneous medium yellow sand; the thickness is about 0.45 m in both cores. Clearly, the sediments of subunits G1 and G2 are of terrigenous origin, deposited in an overall high energy environment, but with phases of alternating low and high energy conditions. Despite the lack of radiocarbon dates, a pre-Holocene age can be inferred.

Unit L occurs in cores P2, P3, P6, P7 and P9 (Figures 6 and 7). It consists of homogeneous grey silty clays with a mean grain-size from 4 to 50 μm; there are some intercalations of coarser material (generally fine sands) in the uppermost part of the unit. χ values are generally low (less than 50 × 10^{-8} m^3/kg) and there is only one peak in core P2, at a depth of 7.85 m, with a value of ca. 100 × 10^{-8} m^3/kg. The carbonate content is generally high, fluctuating between 20% and 40%, with an increase towards the top of the sequence. The organic matter content ranges from 2% to 6% and minor variations occur within the sequence. In the uppermost part

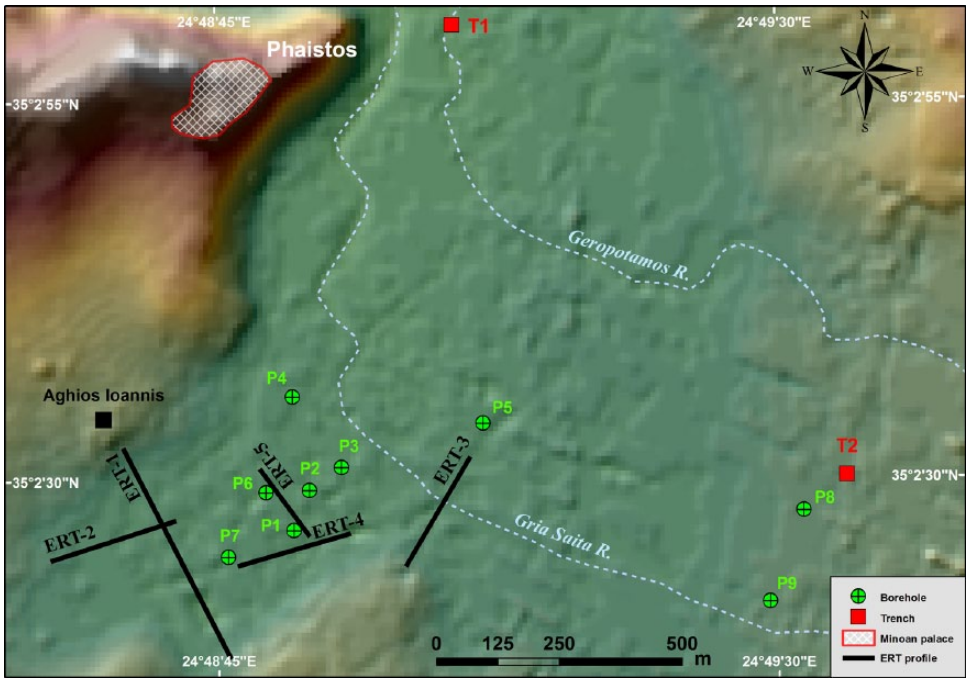

Figure 5. ERT profiles and borehole/trench locations.

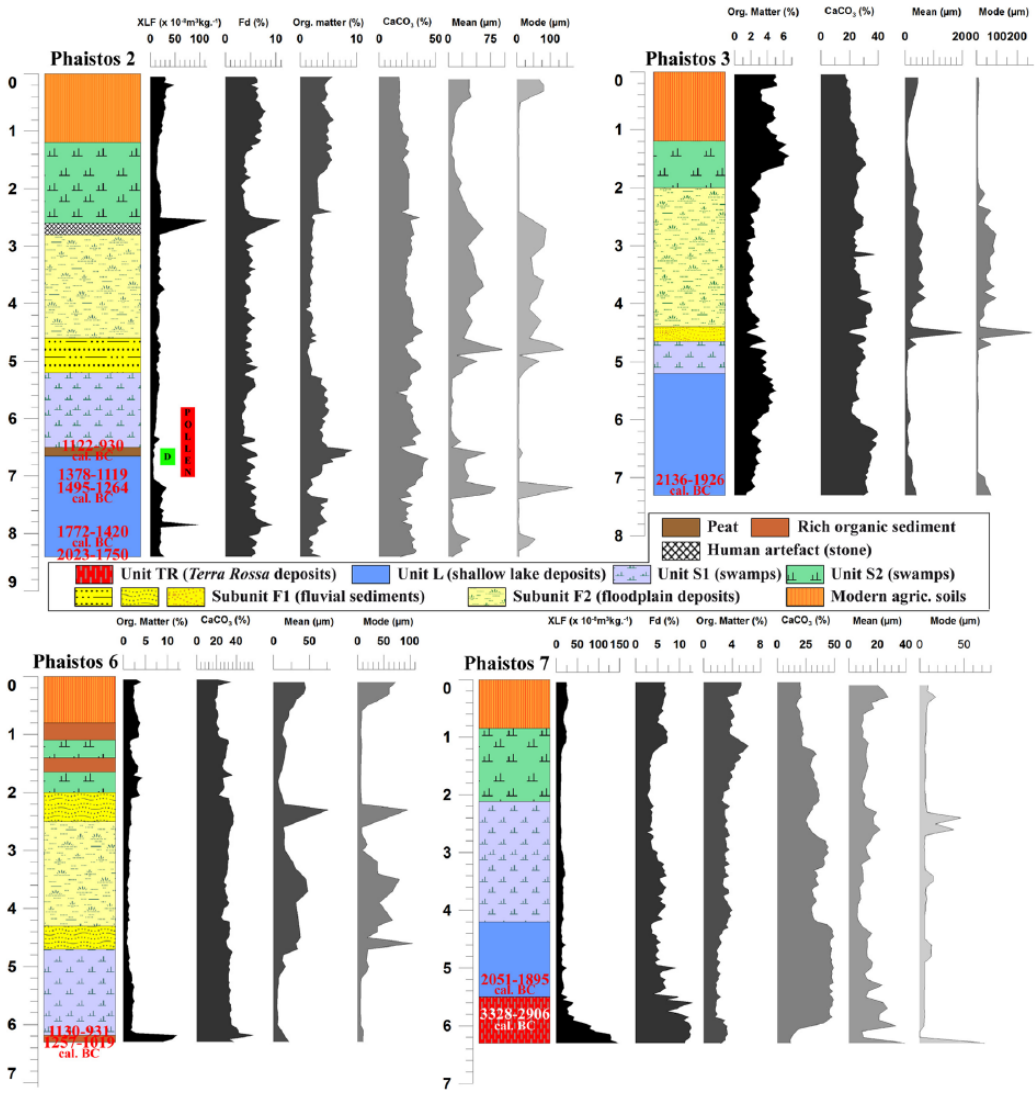

Figure 6. Chronostratigraphy of cores P2, P3, P6 and P7. Magnetic susceptibility parameters (Xlf and Xfd%) are only reported for cores P2 and P7. Organic matter and carbonate content and granulometric indices (mean and mode) are reported for each core, plotted as a function of depth below the surface.

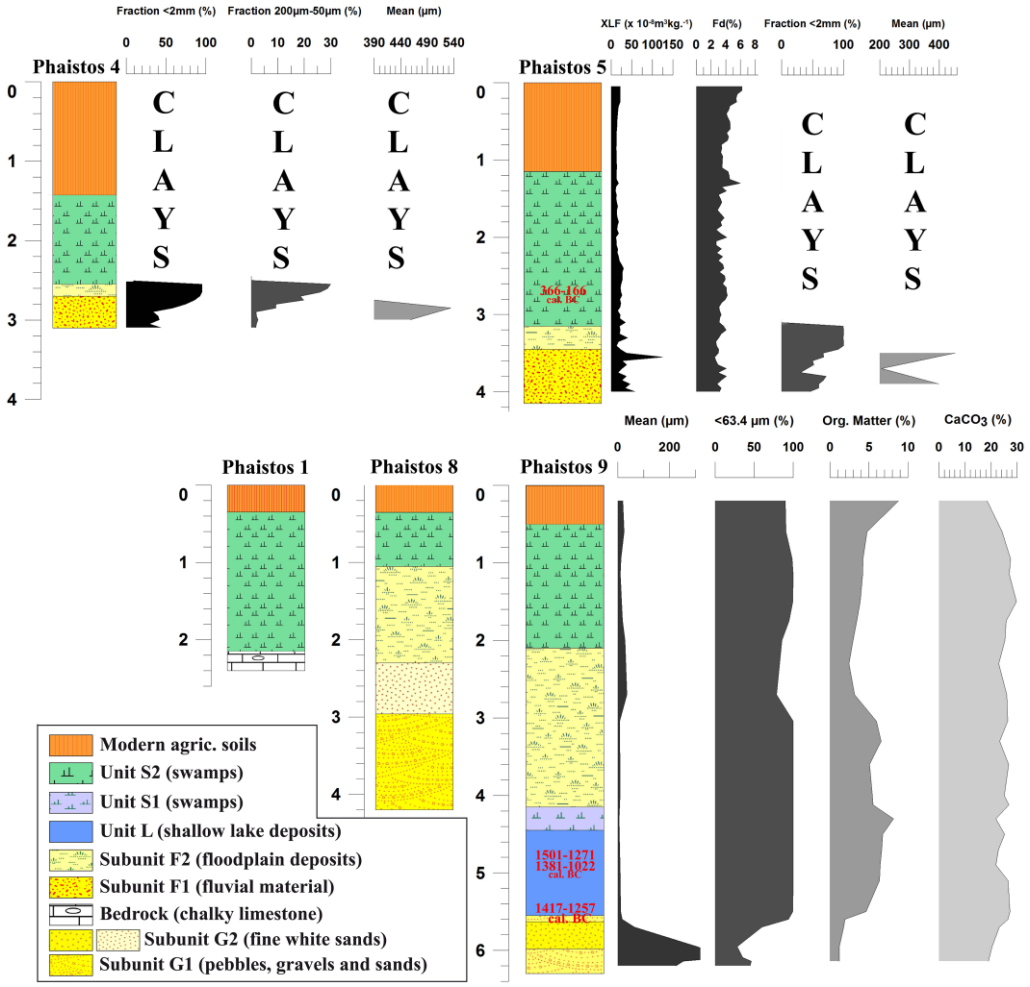

Figure 7. Chronostratigaphy of cores P1, P4, P5, P8 and P9. Magnetic susceptibility parameters (Xlf and Xfd%) are only reported for core P5, while organic matter and carbonate contents and granulometric indexes (mean and mode) are reported for cores P5 and P9, plotted as a function of depth below the surface. For cores P4 and P5, the fractions <2 mm and >2 mm are shown; the mean grain-size was determined solely for the fraction <2 mm.

of the unit, in cores P2 and P6, there is a peat layer (organic matter content of ca. 10%), ca. 10 cm in thickness. Radiocarbon dating of the base of the peat layer in core P6 gave an age of ca. 1257–1019 BC, while the uppermost part in cores P2 and P6 gave the younger age of ca. 1130–930 BC. In core P6, in the lowermost part of the peat deposit, at a depth of 6.35 m, the gastropods *Helicopsis bathytera, Helicella* sp. and *Xerolenta obvia* were identified, which are indicative of terrestrial environments, typically open meadows. Both the presence of the peat and the mollusk assemblage indicate that the water depth was probably decreasing. Clearly, Unit L is older than the age of the peat and this was confirmed by a series of 9 radiocarbon dates performed on plant remains and bulk organic matter. The lowermost part of Unit L was dated to 2024–1750 BC in core P2, and similar ages were obtained for core P3 (2136–1906 BC) and P7 (2051–1895 BC). However, the complete thickness of Unit L remains unknown and deeper coring near cores P2 and P6 would be needed in order to reveal the lowermost part of Unit L. Bioindicators are sparse in Unit L; however, freshwater gastropods, mainly *Planorbia* sp., are present. Diatom analysis (Table 3 and Figure 8(a) and (b)) of the uppermost part of core P2 (from 6.8 to 6.5 m depth), indicated a range of freshwater species (50–65% of the identified species where *Epithemia adnata, Cocconeis placentula, Nitzschia amphibia* and *Synedra ulna* are the most encountered species) and brackish-water species (25–42% of the identified species where *Navicula grimmei, Fallacia pygmaea* and *Tabularia fasciculata* are the most encountered species). Benthic diatoms were the most commonly encountered types within the peat sequence, while a similar amount of benthic and epiphytic diatoms was found within the top of the Unit L (Figure 8(b)). The representation of freshwater species decreases towards the top of Unit L. Haline species of diatoms were also found but with a very low representation (<5%); some authors attribute such a low representation to the presence of migratory birds, which may have come from the nearby sea (in the case of the Messara Plain, Tymbaki Gulf is just 5 km to the west). The diatom results also reveal a gradual increase in brackish-water species towards the peat layer, while at the same time, the freshwater species decrease, indicating a shallowing of the water depth which was probably caused by increased evaporation. Overall, the diatom assemblages indicate the existence of a shallow oligohaline environment during at least Late Minoan times.

Unit S1 occurs above unit L in cores P2, P3, P6, P7 (in the westernmost part of the Messara Plain, in the Phaistos lowlands; Figure 6) and in core P9 (easternmost part of the study area; Figure 7). S1 is well represented in cores P2 and P6 where it overlays the peat layer. Its thickness is greater in cores P2, P3 and P6 (ca. 1.20 m) than in core P7 (<0.50 m) and P9 (0.30 m). The sediments are generally richer in organic matter than in Unit L, with values fluctuating between 4% and 6%, while the carbonate content is around 20% (roughly one-half of the carbonate content of Unit L). The χ values are generally very low (ca. 10×10^{-8} m^3/kg). Bioindicators are scarce, but among them, mollusks found embedded within the sediments are typically from freshwater (swamp) environments.

Table 3. Diatom results obtained for core P2 at the depths of 6.50, 6.60, 6.70 and 6.80 m.

Sample name	Salinity			Habitat			Phaistos_6.80 m		Phaistos_6.70 m		Phaistos_6.65 m		Phaistos_6.60 m		Phaistos_6.50 m	
Specy	Fresh	Brackish	Haline	Epiphytic	Epiphytic and benthic	Benthic	Number	%	Number	%	Number	%	Number	%	Number	%
Achnanthes affinis Ehrenber	x			x			5	1.2	3	0.8	10	2.4			16	3.8
Achnanthes minutissima Ehrenber	x			x							1	0.2				
Amphora coffeieformis Agardh			x			x	26	6.3	9	2.3	13	3.1	2	0.5	4	1.0
Amphora holsatica Hustedt		x				x							11	2.7		
Amphora veneta Hustedt		x				x			36	9.1	8	1.9				
Anomoeoneis sphaerophora (Ehrenberg) Pfitzer		x				x	0	0.0	3	0.8	5	1.2	8	1.9	5	1.2
Caloneis bacillum Ehrenberg		x				x	3	0.7			8	1.9			8	1.9
Cocconeis placentula Ehrenberg	x				x		49	11.8	56	14.2	18	4.3	26	6.3	40	9.6
Craticula cuspidata Kützing		x				x	4	1.0			1	0.2	5	1.2		
Cyclotella meneghiniana Ehrenberg			x			x	5	1.2	9	2.3						
Cymbella affinis Kützing	x			x			1	0.2			20	4.8				
Cymbella cistula (Hemprich) *Grunow*	x			x									11	2.7		
Diploneis ovalis (Hilse) *Cleve*		x			x								1	0.2		
Epithemia turgida (Ehrenberg) *Kützing*	x			x			17	4.1	4	1.0	11	2.6	2	0.5	3	0.7
Epithemia zebra (Ehrenberg) *Kützing/Epithemia adnata (Kützing) Brébisson*	x			x			116	28.0	104	26.4	42	10.0	70	16.9	98	23.5
Fallacia pygmaea (Kützing) Stickle & D G Mann		x				x	4	1.0			46	11.0	36	8.7		
Gomphonema constrictum Ehrenberg		x	x	x					2	0.5						
Gomphonema lanceolatum Ehrenberg		x	x	x			21	5.1					2	0.5	32	7.7
Gomphonema olivaceum Ehrenberg		x	x	x							3	0.7			16	3.8
Gomphonema parvulum Ehrenberg		x	x	x					25	6.3	2	0.5				
Girosigma aff. acuminatum Ehrenberg	x				x						3	0.7				
Mastogloia elliptica Agardh			x			x			3	0.8	9	2.1	6	1.4	5	1.2
Navicula cryptocephala (Agardh) Ehrenberg	x				x						7	1.7				
Navicula grimmei (Hustedt) *Krasske*		x				x	13	3.1			14	3.3	73	17.6	55	13.2
Navicula halophila Grunow		x	x			x	4	1.0							24	5.8
Navicula lanceolata (Agardh) *Ehrenberg*	x					x							3	0.7		
Navicula nivalis Ehrenberg		x				x	1	0.2								
Navicula radiosa Kützing	x					x					13	3.1	16	3.9		
Navicula scalpelliformis Kützing	x					x					1	0.2				
Navicula veneta Kützing	x	x				x			4	1.0	2	0.5	2	0.5		
Nitzschia amphibia Grunow	x					x	47	11.3	68	17.3	105	25.0	87	21.0	40	9.6
Nitzschia commutata Grunow			x			x							8	1.9		
Nitzschia hungarica Grunow			x			x	4	1.0	6	1.5	6	1.4				
Nitzschia linearis W.Smith	x					x	1	0.2								
Nitzschia sigma (Kützing) *W Smith*			x			x									16	3.8
Nitzschia tryblionella Hantzsch		x				x	3	0.7			1	0.2	3	0.7	5	1.2
Rhopalodia gibba (Ehrenberg) *O Muller*		x		x			13	3.1			8	1.9			5	1.2
Rhopalodia gibberula (Ehrenberg) *O Muller*		x				x					5	1.2	5	1.2		
Sellaphora pupula (Kützing) *Mereschkowsky*	x					x					2	0.5	19	4.6		
Surirella ovalis Brébisson			x			x									6	1.4
Synedra ulna (Nitzsche) Ehrenberg	x				x		32	7.7	29	7.4	37	8.8	11	2.7	18	4.3
Tabularia fasciculata Agardh		x				x	46	11.1	33	8.4	19	4.5	7	1.7	21	5.0
Total							415	100	394	100	420	100	414	100	417	100

The most represented species are highlighted in blue (freshwater environments) and in green (brackish environments).

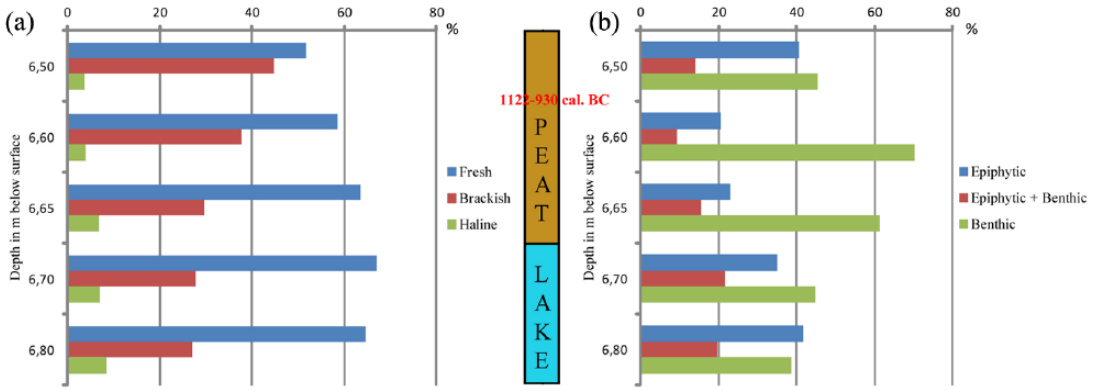

Figure 8. Diatom percentages for core P2 (6.8 to 6.5 m depth): (a) results according to salinity and (b) results according to different habitats.

Gastropods were recognized in core P2: at the depth of 6.07 m, a complete specimen of *Oxyloma elegans* was found, which is indicative of waterlogged conditions, typically living in reeds. Pollen was only found in core P2, from 7 to 5.80 m depth. No radiocarbon dates were obtained for the final stages of Unit S1, but an age of ca. 700 BC can be inferred from the age-depth model for core P2 (Figure 4). Unit S1 is typical of calm environments such as swamps and was deposited from ca. the 11th to the 8th–7th centuries BC. Thus, it is clear that following Minoan Times, a wetland persisted until Ancient Greek times (Archaic period).

Unit F, overlaying unit S1, is found in all cores except P7. It consists of yellowish fine sands to rounded gravels. The thickness of the unit is about 2 m in P9 while in cores P2, P3 and P6 it consists of only 20–40 cm of fine to coarse sands. In cores P4 and P5, a complete thickness was not recovered since a compacted layer of rounded pebbles and gravels prevented deeper drilling. Cores P4, P5 and P9 record the coarsest deposits, while cores P2, P3, P6 and P7 are less influenced by these fluvial sediments. Two subunits are recognized. The sediments of *Subunit F1* were deposited in a high energy environment, which was succeeded in *Subunit F2* by the deposition of floodplain deposits. χ values are generally low in core P2, ca. 20×10^{-8} m^3/kg. However, in core P5 core they are higher and fluctuate within the range of $20–100 \times 10^{-8}$ m^3/kg, which may reflect the input of reworked material from the catchment, in particular from the Asteroussia Mountains where metamorphic rocks, such as gneiss and schists, have a significant magnetic mineral content (Figure 2). Dating Unit F was difficult because of the absence of organic material and thus the age of this fluvial event is difficult to determine accurately; however, it appears to have been a brief episode of alluviation. Based on the radiocarbon dating of core P5 core, and the dated alluvial sequence in both trenches, it is possible that Unit F dates from ca. the 7th to the 5th centuries BC. Clearly, a paleo river existed during the first phases of ancient Greek times; it may have been the modern Gria Saita River (Figure 3) but is also possible it was a former channel of the Geropotamos River, which today flows further north.

Unit S2, above Unit F, a second phase of swamp development can be inferred from all cores. Unit S2 consists of dark grey clays and silts with intercalated peat layers, such as in core P6. The lowermost part of this unit was only dated in core P5, which gave an age of 366–166 BC. (Hellenistic period), while it appears that the uppermost of the unit (close to the surface) is recent (19th to 20th centuries AD).

Chronostratigraphy from the trenches

Trench T1 (lower Phaistos area): Floodplain dynamics. During autumn 2012, a ca. 2 m deep trench was excavated (Table 1; Figure 9(a) and (b)) and sampled for grain-size analyses and radiocarbon dating. It is located at the foothill of the Phaistos site (150 m to the east; Figure 3), at a short distance (less than 20 m) from the present-day main course of the Geropotamos River (dry at that time of the year). Three sedimentary units were identified (Figure 9(a) and (b)) which all reflect the dynamics of terrigenous deposition. Two main phases of low-energy floodplain deposition (yellowish to brownish clays to fine sands) are separated by an intercalated horizon of organic clays. The base of the floodplain sequence is dated to AD 240–AD 391 AD while the uppermost floodplain level is dated to the 20th century AD and forms the modern agricultural soils. Numerous rounded orange pottery sherds were found embedded within the lowermost floodplain layer, indicating a reworked origin. All the results indicate that the Geropotamos River, or one of its former courses, flowed through the area, at least from Late Roman times.

T2 trench (easternmost part of the study area): From limnic to floodplain environments. A second trench was excavated in Spring 2013, to the northeast of cores P8 and P9 (Figure 3). The total thickness of the deposits is about 5.2 m and four main sedimentary units are recognized (Figure 9(c) and (d)). In the lowermost part of T2, dark grey clays occur with similar features to the limnic clays in Unit L, sampled in the lowermost parts of cores P2, P3, P6, P7 and P9. Radiocarbon dating of bulk organic matter from the upper part of these limnic clays gave an age of 896–791 BC and indicates that the area was still a wetland that dried up during Geometric times. Overlying this limnic unit are a sequence of dark to light grey clays and yellowish silts and sands (ca. 50 cm thick), clearly revealing the occurrence of swamp environments (similar to S1 unit). The third sedimentary unit consists of brownish silts to coarse sands and reveals alluvial dynamics, probably the fluvial deposits that are also present in cores P2, P3, P4, P5, P6 and P9. The fourth unit is found 0.30 cm below the modern agricultural soils and consists of organic clays (thickness of about 20 cm). The sedimentary parameters reveal features resembling those of the intercalated organic layer observed in trench T1 that dates to the 19th to 20th centuries AD. In general, the stratigraphy of trench T2 is very similar to that of core P9 (Figure 7, bottom right) in its lower part, and it exhibits similar features to trench T1 in its upper part. Trench T2 provides evidence for the spatial extent of paleolimnic environments eastwards and confirms the ^{14}C dating results for the last stages of the limnic phase, probably around the first third of the first millennium BC.

Pollen results

The pollen results for core P2 reveal vegetation changes from ca. 1250 to 700 BC in the vicinity of Ancient Phaistos (Figure 10). Pollen assemblages evidence an open cultural Mediterranean landscape with a sparse tree cover (Arboreal Pollen (AP) <10%) and a high representation of herbaceous plants related to human activities (ruderal and cultivated plants). Three main local pollen

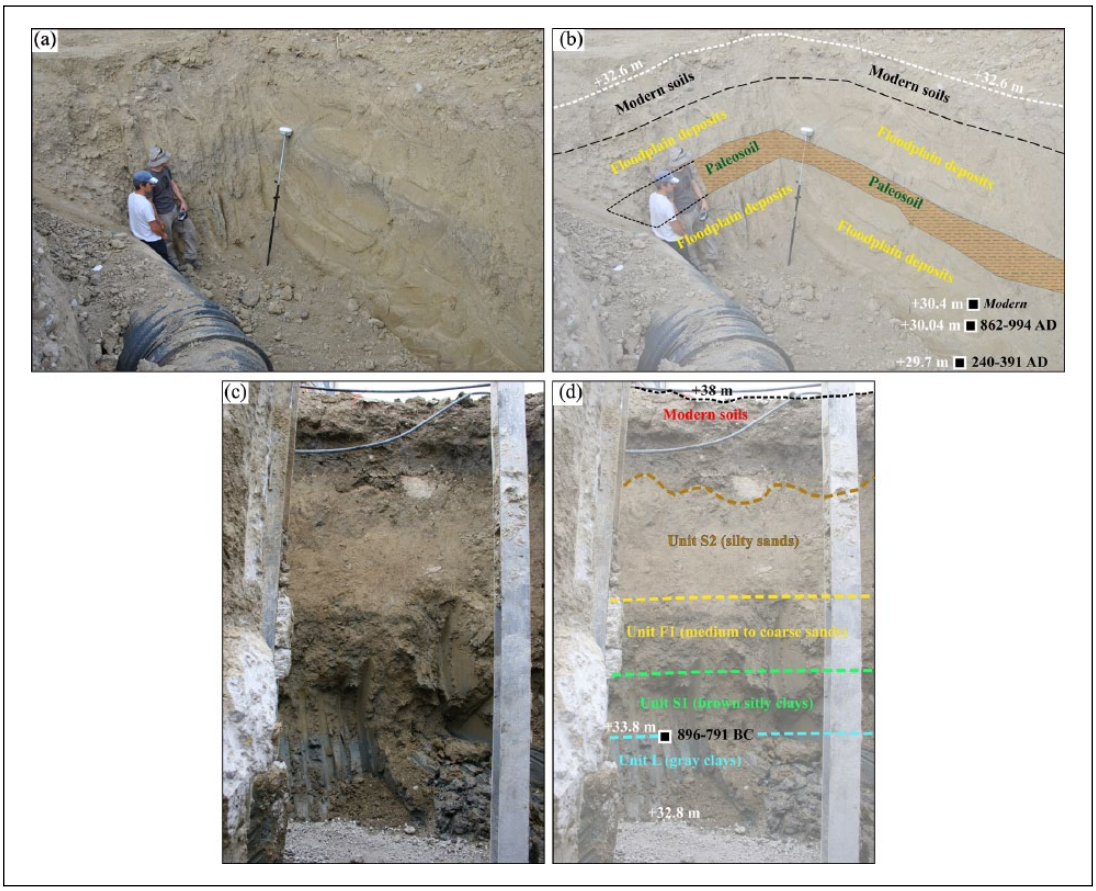

Figure 9. Stratigraphic sections T1 and T2 (a, c) with their paleoenvironmental interpretation and dating (b, d).

areas (LPAZ) were identified based on fluctuations in the pollen curves of ruderal, aquatic and hygrophilous plants: the ruderal assemblage testifies to the evolution of human activities (cultivation and pastoralism) while the others reveal changes in the vegetation composition of the wetland area.

LPAZ1 (700–655 cm, from ca. 1220 ± 71 to ca. 1035 BC, Post-Palatial and Sub-Minoan periods) is characterized by high values of ruderals, *Olea* and aquatics (*Ranunculus*). In the sub-zone *LPAZ1a*, there is an increase in *Ranunculus* values. In the sub-zone *LPAZ1b*, the percentages of *Ranunculus* decrease and, concurrently, there is an increase of the representation of helophytes (*Sparganium* and *Alisma plantago*) and arboreal taxa (*Quercus* sp. and *Pinus brutia*). There is a peak in charcoal particles around 1100–1050 BC, indicating a phase of uncontrolled fires during the Sub-Minoan period or the deliberate burning of human settlements during a period of social instability (Middleton, 2010, 2017).

In *LPAZ2* (650–620 cm, from ca. 1035 to 875 BC, covering the second half of the Sub-Minoan period and the Proto-Geometric period), there is a decrease in ruderals and *Olea*, and Poaceae, *Sparganium* and *Alisma plantago* reach a maximum.

In *LPAZ3* (615–580 cm, from ca 875 to ca. 700 BC, roughly corresponding to the Geometric period), the values of ruderals and *Olea* increase again and the percentages of *Sparganium* and *Alisma plantago* decrease sharply. At the top of the pollen record, *Isoetes* reaches a maximum. This latter species grows in terrestrial rather than aquatic environments, on damp ground (Turland et al., 1993) and it also indicates summer dryness and a wet winter half-year (Bottema and Sarpaki, 2003).

In summary, the pollen data indicate that between the Late Minoan period and the early stages of the Archaic period, a freshwater lake has existed as indicated by the high representation of *Ranunculus* values (LPAZ1a) and became a swamp (after 1000 BC) when the water table declined, as revealed by the decrease in *Ranunculus* (LPAZ1b). The drying up of the lake led to the disappearance of aquatic buttercup and to the extension of helophytic communities (LPAZ2), indicating the settlement of a swampland. The simultaneous peaks in *Isoetes* and of ruderals may reflect an environment disturbed by human activity, and the presence of *Lemna*, at the same time, could indicate a transitory rise in the water table shortly before ca. 700 BC. The intermittent representation of *Alnus glutinosa* and *Tamarix* indicate that an open riparian forest was established around the lake situated in the lowland of Phaistos. It is interesting to point out the absence of *Juglans* and *Platanus*, which today in Greece are frequently encountered in riverine communities. The dynamics of the aquatic and helophytic vegetation confirm the conclusions provided by the sedimentological and diatom analyses. The results generally indicate an open landscape (more so than at other Cretan sites such as Kournas or Chania; Moody et al. (1996) and Bottema and Sarpaki (2003)) along the sequence with very low AP representation with the intermittent presence of *Quercus* and *Pinus* and a very high contribution of pollen from herbs and ruderals (~50–80%). Thus, the results clearly reveal a Mediterranean man-made landscape and environment where trees, mainly *Olea* (domesticated), and herbs and ruderals were highly represented. Similar observations have been recently reported at Palaikastro (Eastern Crete) during Early Minoan times (Cañellas-Boltà et al., 2018).

ERT profiles and subsoil resistivity

The five ERT profiles measured in the western part of the study area (Figures 4 and 11) reveal the subsoil morphology. Three geoelectric units can be identified and are described below.

Unit Ge1. This unit occurs in all profiles, generally within the first few metres. Low resistivity values (<35 Ω m) indicate high conductivity between the present-day surface and a maximum depth of ca. 10–15 m in profile ERT-5, where cores P2 and P6 are

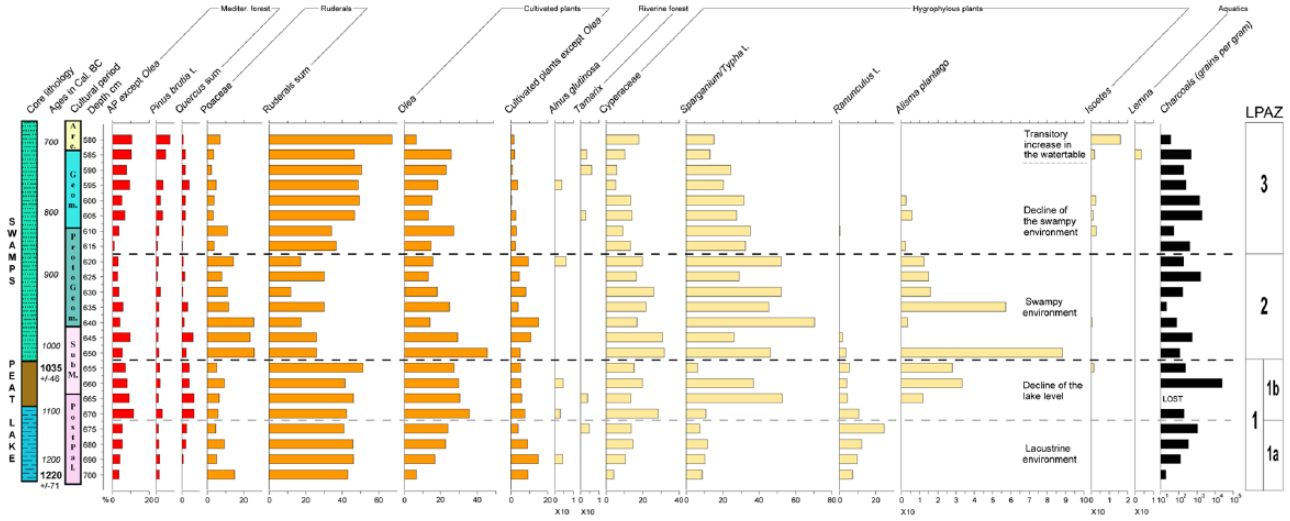

Figure 10. Simplified percentage pollen diagram for Phaistos 2 (5.80–7.00 m depth) together with the lithology, cultural periods (Arc.: Archaic; SubM.: Sub-Minoan) and cal. ^{14}C ages; LPAZ: Local Pollen Assemblage Zone. AP corresponds to the following taxa: *Abies, Alnus glutinosa, Betula, Carpinus betulus, Castanea, Corylus avellana,* Deciduous *Quercus, Fagus, Hedera helix, Ligustrum,* Mediterranean *Quercus, Ostrya* t., *Phillyrea, Pinus brutia* t., *Punica, Tamarix, Ulmus, Vitis*. Ruderal sum corresponds to the following taxa: *Artemisia, Plantago coronopus*, P. *lanceolata, P. major/minor, Aster, Carduus, Carlina, Centaurea solstitialis, Cirsium, Filago, Matricaria, Senecio, Paronychia,* Boraginaceae, *Heliotropium,* Chenopodiaceae, Cichorioideae, *Convolvulus,* Dipsacaceae, *Knautia, Mercurialis annua, Asphodelus, Malva, Polygonum aviculare, Rumex, Galium, Theligonum cynocrambe, Urtica*. Cultivated plants correspond to the following taxa: *Castanea, Punica, Vitis, Acantus, Chrozophora, Cerealia* t., *Secale, Prunus, Carthamus*.

located. The stratigraphy of the latter confirms that fine-grained sediments (mainly clays and fine sands) are associated with the low resistivity. In profile ERT-1, ERT-2 and ERT-4, Unit Ge1 only comprises the first 5 m of the profiles. In profile ERT-4, Unit Ge1 is only 2 to 3 m thick between 117 and 141 m. This is confirmed by the stratigraphy of core P1 where chalky bedrock was reached at the depth of ca. 2.25 m. In some locations, Unit Ge1 may be affected by the presence of the aquifer, resulting in very low resistivity values, as already observed in similar sedimentary contexts (Ghilardi et al., 2015, 2017).

Unit Ge2. This unit has intermediate resistivity values, between 30 and 300 Ω m, and corresponds to unconsolidated coarse sedimentary formations (pebbles, gravels and sands). This material consists of slope debris (colluvial material) derived from the Neogene hills, alluvial deposits (Gria Saita River) or altered substratum. The boundary between Units Ge2 and the overlying Ge1 occurs at different depths: in profile ERT-3, it is at 3–4 m; while in ERT-5, it is at ca. 7–8 m in the middle part of the profile. It appears to be deeper in the NNW part of the profile, probably at more than 10 m. Profile ERT-3 was established across the plain and is situated near the course of the Gria Saita River (from 156–188 mm 35–300 Ω m and likely reflect fluvial deposits comprising very coarse sediments (probably gravels and pebbles) at ca. 5–8 m depth. This is confirmed by the stratigraphy of cores P4 and P5 where at 3–3.5 m depth, there is an impenetrable layer of gravels mixed with coarse sands and pebbles, underlying swampy clays and silts. In profile ERT-2 profile, Unit Ge2 is only found above Unit Ge3, clearly indicating that the resistivity signal reflects the alteration of the bedrock.

Unit Ge3. This unit is only present in profiles ERT-1, ERT-2 and ERT-4, which are mainly located close to the hilly terrain surrounding and to the south of Aghios Ioannis. The resistivity values are very high, between 300 and >2500 Ω m. These values are generally found at depths of at least 5–10 m and below. Profiles ERT-1 and ERT-2 are located close to the village of Aghios Ioannis and extend across the lowlands of the Messara Plain and the gentle slopes of the Kastri Kills. In particular, for ERT-1, the high resistivity values (from 320 to 480 m) close to the surface indicate the presence of the bedrock (chalks) beneath slope debris. Similar observations can be made for profile ERT-2, where colluvial deposits (gravels and pebbles) overlie a high resistivity paleosurface (from 40 to 168 m) at a depth of ca. 7–8 m. Finally, in profile ERT-4, Unit Ge3 has high resistivity values; they occur only from 2 to 3 m below the surface and indicate the position of a bedrock outcrop covered by a thin layer of swamp deposits, as confirmed by the stratigraphy of core P1.

Discussion

Paleogeographic reconstruction of the landscape near Ancient Phaistos

Based on a spatiotemporal interpretation of the ERT profiles, sediment cores and stratigraphic profiles, we now reconstruct the paleoenvironmental evolution of the westernmost part of the Messara Plain for the last 5000 years. We focus especially on the period from ca. 2000 BC to 300 AD (Figures 12–14).

During Neolithic times and the Early Minoan Pre-palatial period (ca. 2500–1900 BC), the landscape configuration is unclear and further coring is needed to sample older sediments. Significant information about the paleolandscape configuration is only available from cores P3, P8 and P9 where the pre-limnic surface was reached: a terrestrial environment with the presence of *Terra Rossa* deposits prevailed to the west until at least 3000 BC (core P3), with a Pleistocene detrital environment to the east (cores P8 and P9). Further studies are needed to date precisely the appearance of the limnic environment. Specifically, deep coring is needed, in the area surrounding cores P2, P3 and P6 to reach bedrock, which may be at the depth of ~12 m, based on the ERT measurements (Figure 11e).

During the Proto-, Neo- and Post-palatial periods (roughly corresponding to 1900–1100 BC; Figure 14, top left), the main feature was the existence of a shallow lake, situated at the foothill of Ancient Phaistos. This aspect of the paleogeographic conditions of the Messara Plain during the Late Holocene conflicts with the interpretation of Fytrolakis et al. (2005), who postulated a possible marine incursion in the lowland of Phaistos palace during Minoan times. The marine layer derived from a core

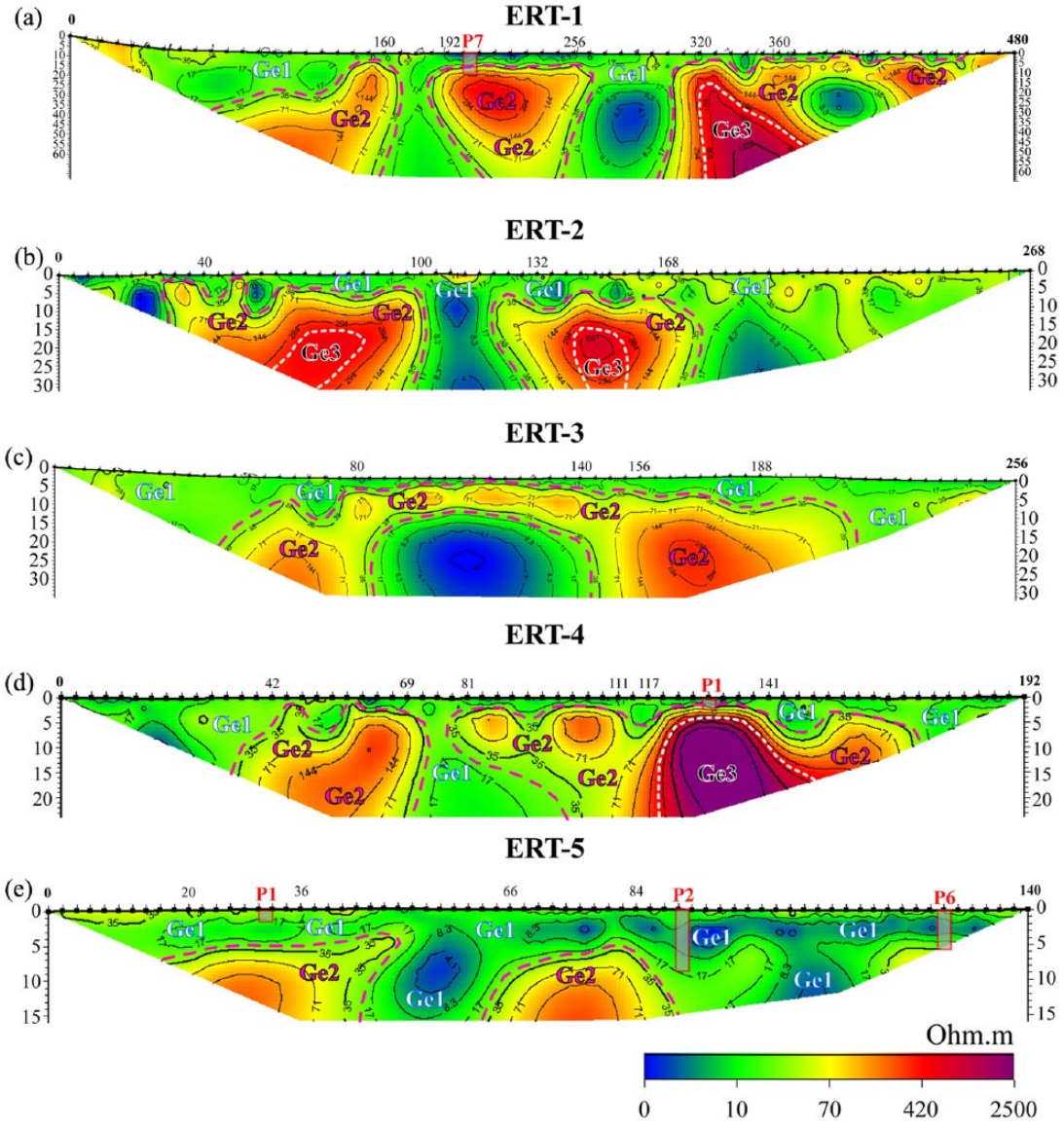

Figure 11. ERT profiles (2D view) and identified geoelectric units (Ge). The location of cores P1, P2, P6 and P7 are reported on the corresponding ERT profile (see Figure 4 for their exact locations).

drilled nearby (Figure 2) and identified at an absolute elevation of ca. 0/+6 m amsl (Fytrolakis et al., 2005) must have been deposited earlier, or during the last post-glacial maximum extent of the sea in the Mediterranean (ca. 6000 cal. kyr BP; Fytrolakis et al., 2005)), or during the last interglacial period (Eemian, ca. 125 kyr BP). During the second millennium BC, our results make clear that the former Minoan palace overhung a freshwater wetland of ca. 1 km^2 in area that reached its maximal extent during the Post-palatial period. This maximal extent is evidenced by the fact that in core P9, the lake environment is only identified for a short interval, dated from ca. 1400–1100 BC. A peak in magnetic susceptibility in core P2, roughly dated to 1700–1500 BC, does not correspond to a tephra deposit (that could presumably have corresponded to the eruption of Santorini and which is recorded elsewhere in Crete; Bottema and Sarpaki, 2003; Lespez et al., 2001; Siart et al., 2010). Rather, it is related to the presence of orange-coloured rounded pottery embedded within the limnic clays; the heated minerals (pottery) are strongly magnetic (Rasmussen, 2001). The origins of this reworked pottery are debatable and could be linked to a period of major disturbance in Crete caused by a series of earthquakes (Monaco and Tortorici, 2003, 2004) or invasions/site collapse (Sandars, 1978). However, there is no direct evidence for an earthquake, or a wave generated by a seismic event since no significant change in the granulometry of the lacustrine deposits (clay to silty clays) was observed; rather, the coring results may suggest a period of heavy precipitation (conceivably generated by the presence of the Santorini eruption ash cloud) within the general context of a humid climate (Macklin et al., 2010), resulting in significant erosion of the hill where Phaistos developed. The origin of the lake formation is debated, and natural (tectonic, climatic, karstic) and anthropogenic factors and/or their combination, may explain this lake development which is only observed elsewhere in Crete during the second millennium BC, at the site of Malia (Figure 1). Indeed, this last Minoan palace located in North Central Crete was probably situated on the eastern margin of a large freshwater wetland during both Neolithic times and the Minoan period (Lespez et al., 2001, 2003).

Subsequently, and probably related to the 3.2 cal. kyr BP dry event, a lake retreat is observed (Figure 14, top right), in particular, in the westernmost part of the Aghios Ioannis lowlands (cores P2, P6 and P7). Despite this sudden climatic change observed in the entire Eastern Mediterranean (Drake et al., 2012), the coring results clearly indicate that the wetland did not dry up completely and isolated ponds remained, especially in the central part of the coring area (core P3 and Trench T2). Sedimentological

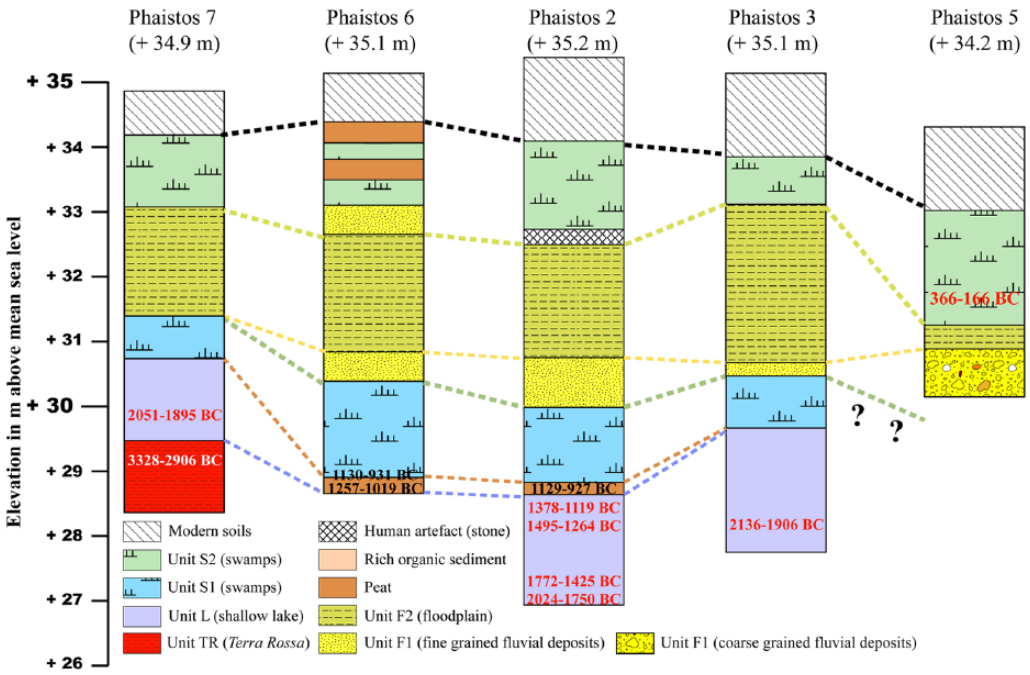

Figure 12. Chronostratigraphic cross-section based on cores P2, P3, P5, P6 and P7.

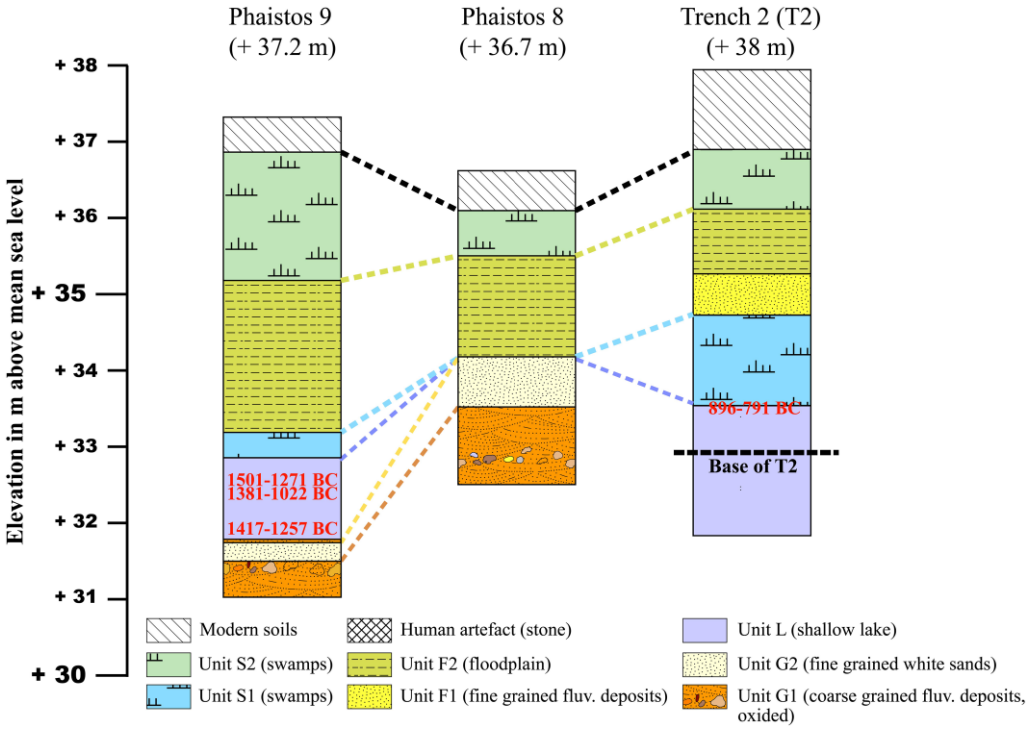

Figure 13. Chronostratigraphic cross-section based on cores P8, P9 and trench T2.

results from trench T2 also clearly reveal the persistence of limnic-swampy environments until the Proto-Geometric and Geometric periods. Due to the drought associated with the 3.2 cal. kyr BP event, the shallow lake (which was probably affected by seasonal droughts causing lowering of the water table during the second millennium BC) was transformed into swampland until approximately the late 8th Century BC (Figure 14, bottom left). The increasing presence of brackish-water diatoms in the last centuries before the 3.2 cal. kyr BP (Figure 8(a)) event suggests strong seasonal evaporation.

Following the wetland environment that prevailed from at least the end of the third millennium to the 8th Century BC, an abrupt input of detrital material occurred from ca. the 7th to the 5th Century BC, locally incising the Minoan-aged lake deposits (Figure 14, bottom right). Dating the first stages of this fluvial sequence is problematic due to the lack of age control on the sediments, and further coring, with additional studies of stratigraphic profiles, could help to date this detrital phase precisely. In particular, ERT-3 profile reveals thick deposits of this coarse alluvial material (several metres; Figure 11c) and deep drilling is needed between cores P3 and P5 to evaluate the complete stratigraphy of the sequence. Climatic conditions reported for the Eastern Mediterranean (Drake, 2012) and Crete, in particular, indicate a phase of drought during the first millennium BC, with fine-grained

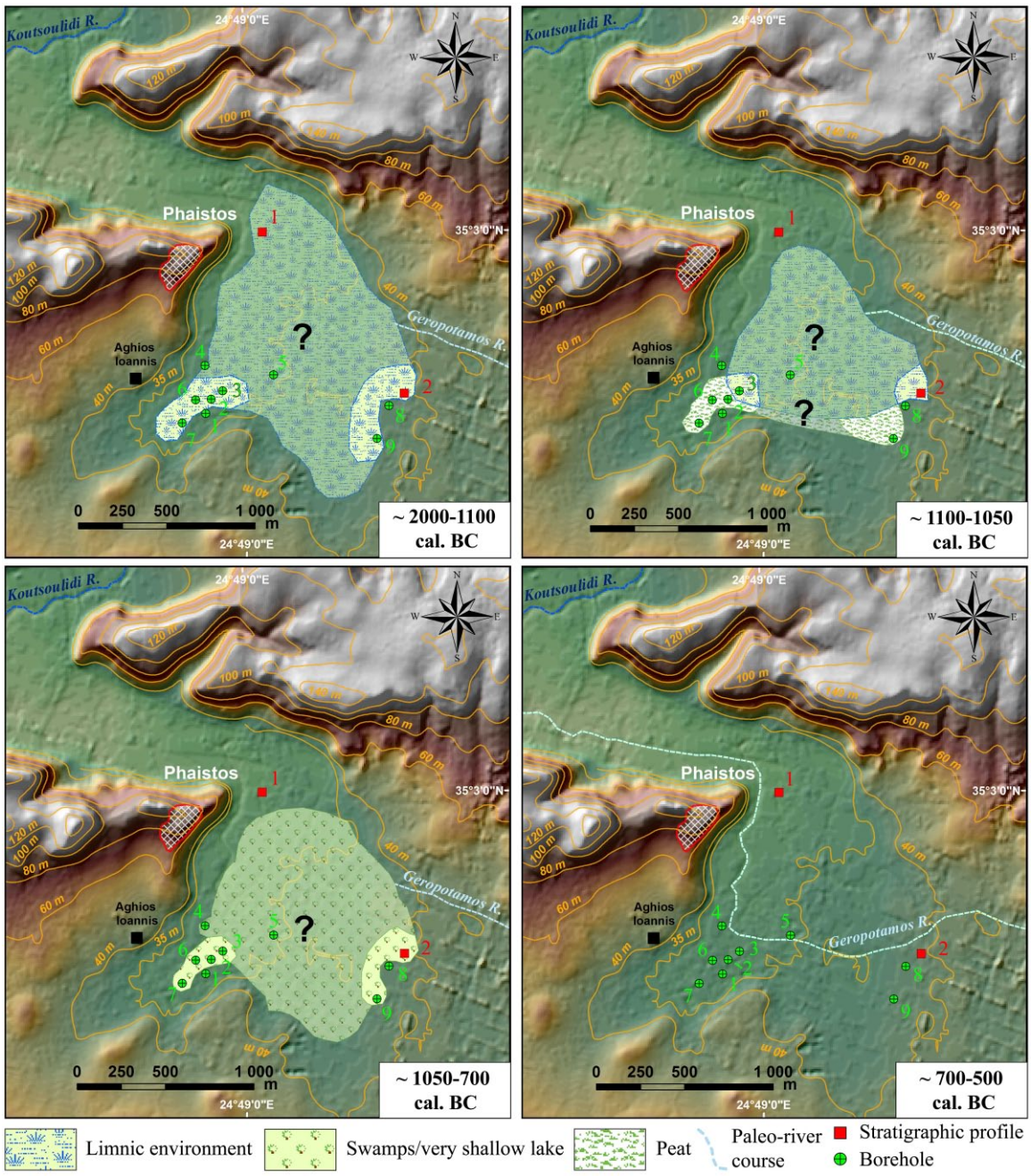

Figure 14. Paleogeographic reconstruction of the westernmost part of the Messara Plain in the vicinity of Ancient Phaistos, from ca. 2200 to 500 cal. BC.

aggradation and general incision of river channels in the Anapodaris River (Macklin et al., 2010).

Following this phase, floodplain deposits from the Gria Saita River influenced the morphology of the area during Roman times and probably until the Ottoman period (Figure 9(a) and (b)).

The Western Messara Plain: Long-term history of complex human–environment interactions?

An initial question is the origin of the shallow lake that formed at the foothill of Phaistos. Indeed, climate reconstructions for the Eastern Mediterranean, and Crete in particular, suggest that from ca. 2400 ± 200 BC to AD 600 ± AD 100, colder and drier conditions prevailed within the region (Finné, 2011, 2014; Theodorakopoulou et al., 2012). However, some authors consider that the second millennium BC was a period of intense flooding with major river alluviation (Macklin et al., 2010), comparable to the medieval 'Little Ice Age' (Moody, 2000). Despite the general context of supposed dry climatic conditions, our dataset demonstrates that a shallow lake developed at the foothill of Phaistos and existed until the first third of the first millennium BC. The existence of a lake can be regarded as indicating generally wet conditions, and the chronostratigraphic results presented herein clearly indicate that the 2nd millennium BC in South-Central Crete (Phaistos area) was a period of mild climatic conditions. Due to the vicinity of the Ida and Asteroussia mountain ranges, composed in part of carbonate rocks (limestones and Miocene chalks; Figure 2), karstic phenomena, coupled with local strong tectonic activity (a locally reinforced subsidence phenomenon) could also be evoked to explain the creation of the Minoan shallow lake. The tectonic factor seems to have played a major role in the formation of the lake, since the level of the lake deposits, dated to ca. 1200 BC in cores P2, P3 and P6, is at an elevation of ca. +28.5 m amsl, while in cores P7 and P9 (which are both on

the margins of the paleolake), it is at ca. +30.5 m and + 32.5 m amsl, respectively. However, this subsidence was also clearly influencing the course of the Geropotamos River during the first millennium BC (Figure 14, bottom right) when the lake dried up: instead of flowing westwards, directly to the outlet towards Tymbaki Gulf, it seems that the river flowed just below Aghios Ioannis, after an interval of meandering. One also may ask whether human actions were responsible for the formation of the wetland; although, this issue is difficult to resolve there are case studies of human actions directly interfering with the natural course of streams in Greece, during the Late Bronze Age. Advanced land reclamation techniques are mainly documented in the Mycenaean world. At Tyrins (Peloponnesus, Greece), a 300-m-long and 10-m-high dam was built in ca. 1250–1200 BC (Late Helladic times) to prevent catastrophic flooding affecting the lower part of the Mycenian site (Balcer, 1974). In Crete, at Zakros-Choiromandres (in the east of the island; Figure 1), there is evidence of the hydraulic control of local streams during the Early Proto-Palatial period (1900–1700 BC) to protect arable land from flooding and erosion (Vokotopoulos et al., 2014). Similar dams and protecting walls have been observed on Pseira Island, North Central Crete (Betancourt, 2012) and an important collecting system for water irrigation purposes was also proposed at Malia (East Central Crete) for the same period (Müller Celka et al., 2014). Were the Minoans, at the beginning of Proto-Palatial period, capable of building a dam to retain a large volume of freshwater at the narrowest part the Geropotamos valley, just below the Phaistos site? Archaeological evidence is lacking to test this possibility, but clearly the Late third millennium BC corresponds to the main building phase of palaces in Crete (Alexiou, 1980) and it could also have been linked to the agricultural development of the Messara Plain that was controlled by Phaistos. Future archaeological and geophysical research is needed to evaluate the potential existence of a paleodam and hydraulic structures close to Phaistos that could have impounded the water in the lowlands of the western Messara Plain.

The question of the lake drying up is also debatable: Was it drained for agricultural purposes? Another point is the detrital input (directly related to the lake drying up) recorded around the mid-first millennium BC, occurring approximately where the modern course of the Gria Saita River is located. Clearly, the complete drying up of the Minoan lake and of the later swamps contributed to modify the topography and configuration of the hydrographic network, probably after the 8th Century BC. During the second millennium and the first centuries of the first millennium BC, intermittent streams and rivers, such as the paleoGeropotamos and paleoGria Saita, probably terminated in the eastern and northern margins of the paleolake (Figure 14, top left), which locally controlled the rivers' base level. Clearly, after the 8th Century BC, most of the streams and rivers from the western Messara Plain terminated in Tymbaki Gulf. Recent paleoclimate studies conducted in the Eastern Mediterranean (Bar-Matthews et al., 2003; Psomiadis et al., 2018) and regional paleofluvial research conducted in Crete (Macklin et al., 2010) have confirmed a period of high aridity during the mid-first millennium BC. This last date corresponds to the phase of alluvial input following the lake sequence and one of the possible consequences of the arid climatic conditions observed during the Archaic period could have been the development of incision (of the lake deposits) and catastrophic floods. Nevertheless, an anthropogenic channel modification of the Geropotamos river course is possible and it has been observed elsewhere in Crete (Theodorakopoulou and Bassiakos, 2017). The aim of the river channelization during Early Greek times would have been to drain the wetland and to reclaim the area for agricultural purposes during a flourishing period (development of the Greek *Poleis*).

On the possible identification of the 3.2 cal. kyr BP RCC event around ancient Phaistos and its consequences

The coring results and the pollen sequence from core P2 reveal an important lake retreat (indicated by 0.10 cm of peat accumulation) around the 12th-11th Centuries BC, which was clearly linked to a short but severe climatic oscillation (drought), probably not exceeding a century in duration. It confirms other research conducted in the Eastern Mediterranean (Drake et al., 2012) which highlights a severe drought at the end of the Bronze Age (~1200–1100 BC). Several studies also proposed that one of the major consequences of the 3.2 cal. kyr BP was the collapse of Mediterranean Bronze Age civilizations (Kaniewski et al., 2015; Tsonis et al., 2010), or at least an important change in agricultural practices (Kaniewski et al., 2013). The 3.2 cal. kyr BP event has its origins in climatic shifts from the North Atlantic to the Mediterranean area (Fletcher and Zielhofer, 2013), with a distinct increase in winter precipitation and summer aridity (Kuhnt et al., 2008). However, this resulted in diverse impacts in areas around the Mediterranean Sea, including an increase in humidity indices in the north-eastern Aegean Sea (Glais et al., 2017; Psomiadis et al., 2018). These contradictory findings of both arid and humid trends have triggered various discussions, for example, of the effect of both climatic oscillations and the intensification of human land-use (Roberts et al., 2011; Marinova et al., 2012; Weiberg et al., 2016).

Our dataset, based on the first pollen sequence obtained from the vicinity of a Minoan palace and spanning the Late Minoan to the Archaic period, indicates no major change in the type of agriculture: olive trees and cultivated plants are still present (Figure 10), reflecting the continuous occupation of the surroundings of Phaistos, despite the decline of the Minoan civilization. A slight decrease in the pollen representation of *Olea* and ruderals is however observed during the 10th to 9th centuries BC (Proto-Geometric period), together with a sharp decrease in the concentration of charcoal particles. However, the representation of the other cultivated plants remains stable. These results may indicate a reduced human presence in the surroundings of Ancient Phaistos during a period of socio-cultural instability. However, the results of this study make it clear that the so-called 3.2 cal. kyr BP RCC event had little impact on the settlement history of the Western Messara Plain and cannot be used as evidence for a potential collapse of the Minoan civilization in the Phaistos area.

Conclusion

Paleoenvironmental and geophysical research conducted in the vicinity of Ancient Phaistos reveals for the first time the landscape configuration from Minoan to Roman times in the lowland of the palace. The results highlight the existence of a shallow freshwater lake from, at least, the Late third millennium to the Late 2nd millennium BC (roughly corresponding to the Proto-, Neo- and Postpalatial periods). In addition, wetland environments (swamps) prevailed during the proto- and neo-palatial Minoan periods and probably until the Early Archaic period. From a geo-archaeological perspective, our results make clear that Phaistos was not located on the seashore of a paleo-extended Tymbaki Gulf during Late Holocene (4.2-0 kyr BP), as suggested previously. This conclusion is supported by diatom and pollen analysis of specific layers, and our work confirms the archaeological evidence that placed Phaistos at some distance from the coastline during Minoan times: Kommos and Matala probably served as harbours for importing and exporting goods. Ancient Phaistos overhung a shallow lake that reached its maximum extent around the 15th to 12th centuries BC covering an area of at least 1 km^2. The wetland was affected by a severe drought probably caused by the 3.2 cal. kyr BP RCC event and our work confirms the findings

of other regional paleoclimatic research in the Eastern Mediterranean. Despite the lake retreat, which was mainly controlled by climatic factors at the end of the Minoan times, it did not disappear completely and several ponds/swampy areas persisted until the 8th Century BC. A combination of particular tectonic (local subsidence), karstic and climatic conditions is possible to explain the formation of the Lake. Subsequently, during Ancient Greek and Roman times, fluvial dynamics shaped the westernmost margin of the Messara Plain thanks to more arid climatic conditions. Our pollen record, which spans the period from Late Minoan times and the early stages of the Archaic period, provides no evidence of an abrupt and complete abandonment by the local population and major changes in agricultural practices due to the 3.2 cal. kyr BP RCC event, even if during Proto-Geometric times (a period of high socio-cultural instability that occurred at ca. 970–810 BC) a reduced human presence near Phaistos is attested. The rich paleoecological dataset presented herein makes it clear that the regional-scale Late Bronze Age drought was not responsible for the collapse of Minoan civilization in the vicinity of Phaistos, one of the most important palaces. Our study exemplifies the utility of a multidisciplinary paleoenvironmental approach which elucidates the relationships between landscape dynamics and human occupation in South-Central Crete. Our findings now need to be considered by archaeologists and historians in subsequent reconstructions of the socio-cultural evolution of the Phaistos site, and in the westernmost part of the Messara Plain, from Minoan to Roman times.

Acknowledgements

The work was made possible by an agreement with the Phaistos Project, a survey programme jointly established between the University of Salerno (Italy) and the Ephoria of Antiquities (Heraklion, Crete, Greece) under the aegis of the Italian Archaeological School in Athens (Greece). Facilities provided by the *Ecole française d'Athènes* (Dir. Alexandre Farnoux) and the Italian School of Archaeology in Athens (Dir. Emmanuel Greco) are greatly appreciated. Special thanks are due to Jordi Revelles (UAB, Barcelona, Spain) and Florence Sylvestre (CEREGE, France) for fruitful discussions and for providing valuable help. The authors thank Jan Bloemendal for improving the English and two anonymous referees for fruitful remarks. Finally, they would like to dedicate this article to the memory of Dr Françoise Gasse and Professor Oliver Rackham.

Funding

This article is a contribution of the DIKIDA research programme, funded by the ANR (Espace et territoire 2010, ANR-10-ESVS-011-02) and directed by Daniela Lefevre-Novaro (University of Strasbourg, France) for archaeological investigations, and by Matthieu Ghilardi (CNRS, France) for the paleoenvironmental studies.

References

Alexiou S (1980) La civilisation minoenne. Heraklion Crete Publisher, 136 pp.

Balcer JM (1974) The Mycenaean dam at Tyrins. *American Journal of Archaeology* 78(2): 141–149.

Bar-Matthews M, Ayalon A, Gilmour M et al. (2003) Sea-land oxygen isotopic relationships from planktonic foraminifera and speleothems in the Eastern Mediterranean region and their implication for paleorainfall during interglacial intervals. *Geochimica et Cosmochimica Acta* 67(17): 3181–3199.

Battarbee RW, Jones VJ, Flower RJ et al. (2001) Diatoms. In: Last WM and Smol JP (eds) *Tracking Environmental Change using Lake Sediments*. Dordrecht: Kluwer Academic Publishers, pp. 155–202.

Beauvais A, Parisot J-C and Savin C (2007) Ultramafic rock weathering and slope erosion processes in a south West Pacific tropical environment. *Geomorphology* 83(1–2): 1–13.

Bengtsson L and Enell M (1986) Chemical analysis. In: Berglund BE (ed.) *Handbook of Holocene Palaeoecology and Palaeohydrology*. Chichester: John Wiley & Sons, pp. 423–451.

Betancourt PP (2012) *The Dams and Water Management Systems of Minoan Pseira*. Philadelphia, PA: INSTAP Academic Press.

Beug HJ (2004) *Leitfaden der Pollenbestimmung für Mitteleuropa und angrenzende Gebiete*. München: Verlag Dr. Friedrich Pfeil.

Bintliff JL (1977) Natural environment and human settlement in Prehistoric Greece based on original fieldwork: Part 2. *British Archaeological Reports* 2(Suppl. 28): 734.

Blaauw M (2010) Methods and code for 'classical' age-modelling of radiocarbon sequences. *Quaternary Geochronology* 5: 512–518.

Bottema S and Sarpaki A (2003) Environmental change in Crete: A 9000-year record of Holocene vegetation history and the effect of the Santorini eruption. *The Holocene* 13(5): 733–749.

Bredaki M, Longo F and Benzi M (2009) Progetto Festòs. Ricognizioni archeologiche di superficie: le campagne 2007-2009. *ASAtene* 87(serie III, 9): 935–978.

Bredaki M and Longo F (in press) Phaistos survey project: From the Minoan Palace to the Classical and Hellenistic Town. In: *11th International Cretological Congress*, Rethymno, 21–27 October 2011.

Bredaki M, Longo F and Benzi M (2012) Phaistos Project: Preliminary result of the 2009-2010 Survey Campaigns. In: Andrianakis M, Varthalithou P and Tzachili I (eds) *Archaeological Work in Crete 2* (Proceedings of the 2nd Meeting, Rethymno). Rethymno: Faculty of Letters Publications, University of Crete, pp. 274–282.

Bryson RA, Lamb HH and Lonley DL (1974) Drought and decline of Mycenae. *Antiquity* 48(189): 46–50.

Buurman P, de Boer K and Pape T (1997) Laser Diffraction grain-size characteristics of Andisols in perhumid Costa Rica: The aggregate size of allophane. *Geoderma* 78: 71–91.

Buurman P, Pape T and Muggler RCC (1996) Laser grain-size determination in soil genetic studies: Practical problems. *Soil Science* 162: 211–218.

Cañellas-Boltà N, Riera-Mora S, Orengo HA et al. (2018) Human management and landscape changes at Palaikastro (Eastern Crete) from the Late Neolithic to the Early Minoan period. *Quaternary Science Reviews* 183: 59–75.

Carbone F (2017) La monetazione in bronzo di Festòs. In: De Caro S, Longo F, Scafuro M et al. (eds) *Percorsi. Scritti di e per Angela Pontrandolfo, vol. 2*. Paestum: Pandemos, pp. 151–161.

Carbone F (in press) Overstrikes at Phaistos: Chronologies and flow, in *Archaeological Work in Crete* 4, Rethymno.

Carpenter R (1966) *Discontinuity in Greek Civilization*. Cambridge: Cambridge University Press, 79 pp.

Casford JSL, Rohling EJ, Abu-Zied RH et al. (2003) A dynamic concept for eastern Mediterranean circulation and oxygenation during sapropel formation. *Palaeogeography, Palaeoclimatology, Palaeoecology* 190: 103–119.

Dean WE (1974) Determination of carbonate and organic matter in calcareous sediments and sedimentary rocks by loss on ignition: Comparison with other methods. *Journal of Sedimentary Petrology* 44: 242–248.

Dearing JA, Dann RJL, Hay K et al. (1996) Frequency-dependent susceptibility measurements of environmental materials. *Geophysical Journal International* 124(1): 228–240.

Di Tonto S (2009) Considerazioni preliminari sulla ceramica neolitica dei recenti scavi di Festòs. *Atti dei Convegni dei Lincei* 173: 309–354.

Drake BL (2012) The influence of climatic change on the Late Bronze Age Collapse and the Greek Dark Age. *Journal of Archaeological Science* 39(6): 1862–1870.

Farr TG, Rosen PA, Caro E et al. (2007) The Shuttle Radar Topography Mission. *Review of Geophysics* 45: RG2004.

Fassoulas C (2001) The tectonic development of a Neogene basin at the leading edge of the active European margin. The Heraklion basin, Crete, Greece. *Journal of Geodynamics* 31: 63–84.

Finné M, Bar-Matthews M, Holmgren K et al. (2014). Speleothem evidence for late Holocene climate variability and floods in Southern Greece. *Quaternary Research* 81(2): 213–227.

Finné M, Holmgren K, Sundqvist HS et al. (2011) Climate in the eastern Mediterranean, and adjacent regions, during the past 6 000 years — a review. *Journal of Archaeological Science* 38: 3153–3173.

Fletcher WJ and Zielhofer C (2013) Fragility of Western Mediterranean landscapes during Holocene rapid climate changes. *Catena* 103: 16–29.

Fytrolakis N, Peterek A and Schröder B (2005) Initial geoarchaeologic Investigations on the Holocene Coastal Configuration near Phaistos/Ayia Triada (Messara Plain, Central Crete, Greece). In: Fouache E and Pavlopoulos K (eds) *Sea-Level Changes in Eastern Mediterranean during the Holocene* (Zeitschrift für Geomorphologie Suppl. 137). Stuttgart: Schweizebart Science Publishers, pp. 111–123.

Ghilardi M, Istria D, Curras A et al. (2017) Reconstructing the landscape evolution and the human occupation of the Lower Sagone River (Western Corsica, France) from the Bronze Age to the Medieval period (ed M Ghilardi and L Lespez; *Geoarchaeology of the Mediterranean islands*). *Journal of Archaeological Science: Reports* 12: 741–754.

Ghilardi M, Sanderson D, Kinnaird T et al. (2015) Dating the Bridge at Avignon (South France) and reconstructing the Rhone River fluvial palaeo-landscape in Provence from Medieval to Modern times. *Journal of Archaeological Science: Reports* 4: 336–354.

Glais A, Lespez L, Vannière B et al. (2017) Human-shaped landscape history in NE Greece. A palaeoenvironmental perspective. *Journal of Archaeological Science: Reports* 15: 405–422.

Gogou A, Bouloubassi I, Lykousis V et al. (2007) Organic geochemical evidence of Late Hlacial-Holocene climate instability in the north Aegean sea. *Palaeogeography, Palaeoclimatology, Palaeoecology* 256(1–2): 1–20.

Kaniewski D, Guiot J and Van Camp E (2015) Drought and societal collapse 3200 years ago in the Eastern Mediterranean: a review. *Climate Change* 6(4): 369–382.

Kaniewski D, Van Campo E, Guiot J et al. (2013) Environmental roots of the late Bronze Age Crisis. *PLoS ONE* 8(8): e71004.

Kelletat D and Zimmermann L (1991) Verbreitung und Formtypen rezenter und subrezenter organischer Gesteinsbildungen an den Küsten Kretas. *Essener Geographische Arbeiten* 23: 1–164.

Krammer K and Lange-Bertalot H (1986) Bacillariophyceae. 1. Teil: Naviculaceae. In: Ettl H, Gerloff J, Heynig H et al. (eds) *Süsswasser flora von Mitteleuropa* (Band 2/1). Stuttgart; New York: Gustav Fischer Verlag, 876 pp.

Krammer K and Lange-Bertalot H (1988) Bacillariophyceae. 2. Teil: Bacillariaceae, Epithemiaceae, Surirellaceae. In: Ettl H, Gerloff J, Heynig H et al. (eds) *Süsswasserflora von Mitteleuropa* (Band 2/2). Jena: VEB Gustav Fischer Verlag, 596 pp.

Krammer K and Lange-Bertalot H (1991a) Bacillariophyceae. 3. Teil: Centrales, Fragilariaceae, Eunotiaceae. In: Ettl H, Gerloff J, Heynig H et al. (eds) *Süsswasserflora von Mitteleuropa* (Band 2/3). Stuttgart; Jena: Gustav Fischer Verlag, 576 pp.

Krammer K and Lange-Bertalot H (1991b) Bacillariophyceae. 4. Teil: Achnanthaceae, Kritische Ergänzungen zu Navicula (Lineolatae) und Gomphonema, Gesamtliteraturverzeichnis Teil 1-4. In: Ettl H, Gerloff J, Heynig H et al. (eds) *Süsswasserflora von Mitteleuropa* (Band 2/4). Stuttgart; Jena: Gustav Fischer Verlag, 437 pp.

Kuhnt T, Schmiedl G, Ehrmann W et al. (2007) Deep-sea ecosystem variability of the Aegean Sea during the past 22kyr as revealed by Benthic Foraminifera. *Marine Micropaleontology* 64: 141–162.

Kuhnt T, Schmiedl G, Ehrmann W et al. (2008) Stable isotopic composition of Holocene benthic foraminifers from the Eastern Mediterranean Sea: Past changes in productivity and deep water oxygenation. *Palaeogeography, Palaeoclimatology, Palaeoecology* 268: 106–115.

La Rosa V (1985) Preliminary considerations on the problem of the relationship between Phaistos and Haghia Triada (*A Great Minoan Triangle in South-Central Crete: Kommos, Haghia Triada, Phaistos)*. *Scripta Mediterranea* 6: 45–54.

La Rosa V (1990) Ceramiche ellenistiche da Festòs: per il problema della distruzione finale della città. In: *B' Epistimonikì Sinàntisi yia tin ellinistiki keramikì – Praktikà (Rodi, marzo 1989)*, Atene, pp. 160–166.

La Rosa V (1992a) Agia Triada. In: Myers JW, Myers EE and Cadogan G (eds) *The Aerial Atlas of Ancient Crete*. London: Thames & Hudson, pp. 70–77.

La Rosa V (1992b) Phaistos. In: Myers JW, Myers EE and Cadogan G (eds) *The Aerial Atlas of Ancient Crete*. London: Thames & Hudson, pp. 232–243.

La Rosa V (2010) Ayia Triada. In: Cline EH (ed.) *The Oxford Handbook of the Bronze Age Aegean (ca. 3000–1000 BC)*. Oxford: Oxford University Press, pp. 495–508.

Lefevre-Novaro D, Martzloff L and Ghilardi M (2015) Géosciences, archéologie et histoire en Crète de l'Âge du Bronze récent à l'époque Archaïque. In: *Proceedings of the Colloquium DIKIDA*, Strasbourg, 16–18 october 2013. Padova: Aldo Ausilio editore, Bottega d'Erasmo, p. 388.

Lespez L, Dalongeville R, Pastre JF et al. (2001) Le site de Malia et la mer, approche paléoenvironnementale. Résultats préliminaires: l'analyse du sondage VI. *Topoi* 11(2): 613–633.

Lespez L, Dalongeville R, Pastre JF et al. (2003) Middle-Late Holocene palaeo-environmental evolution and coastline changes of Malia (Crete). In: Fouache E (ed.) *The Mediterranean World Environment and History* (Collection Environment). Paris: Elsevier, pp. 439–452.

Loke MH (2003) *RES2DINV, Rapid 2-D Resistivity and IP Inversion Using the Least-Square Method* (Geotomo Software User's Manual). Singapore: Geotomo Software, 123 pp.

Longo F (2015a) Considerazioni preliminari sulla topografia della città greca di Festòs. In: Lefèvre-Novaro D, Martzolff L and Ghilardi M (eds) *Géosciences, Archéologie et Histoire en Crète de l'âge du Bronze récent a l'époque archaÏque*. Padua: La Bottega d'Erasmo, pp. 159–182.

Longo F (2015b) Phaistos Project. The Greek polis in the light of recent topographic studies. In: Karanastasi P, Tzigounaki A and Tsigounaki C (eds) *Archaeological Work in Crete* (AEK 3 2013). Rethymno: Faculty of Letters Publications, University of Crete, pp. 465–481.

Longo F (in press) The fortification walls of Phaistos: some preliminary considerations. *ASAtene*.

Maas GS and Macklin M (2002) The impact of recent climate change on flooding and sediment supply within a Mediterranean mountain catchment, Southwestern Crete, Greece. *Earth Surface, Processes and Landforms* 27(10): 1087–1105.

Macklin MG, Tooth S, Brewer PA et al. (2010) Holocene flooding and river development in a Mediterranean steepland catchment: The Anapodaris Gorge, South Central Crete, Greece. *Global and Planetary Change* 70: 35–52.

Macklin MG, Benito G, Gregory KJ et al. (2006) Past hydrological events reflected in the Holocene fluvial record of Europe. *Catena* 66: 145–154.

Marangou L (1992) *Minoan and Greek Civilization from the Mitsotakis Collection*. Athens: The Nicholas P. Goulandris Foundation, Museum of Cycladic Art, p. 26.

Marginesu G (in press) Le fonti letterarie ed epigrafiche. In: Longo F and Greco A (eds) *Festos 1*. Athens: Monografie SAIA.

Marino G (2008) *Paleoceanography of the Interglacial Eastern Mediterranean Sea* (LPP Foundation Contribution Series 24). Utrecht: LPP Foundation, 145 pp.

Marino G, Rohling EJ, Rijpstra WI et al. (2007) Aegean Sea as driver of hydrological and ecological changes in the eastern Mediterranean. *Geology* 35: 675–678.

Marinova E, Tonkov S, Bozilova E et al. (2012) Holocene anthropogenic landscapes in the Balkans: The palaeobotanical evidence from southwestern Bulgaria. *Vegetation History and Archaeobotany* 21: 413–427.

Mayewski PA, Rohling EJ, Stager JC et al. (2004) Holocene climate variability. *Quaternary Research* 62: 243–255.

Mentesana R, Amato V, Day P et al. (2016) Looking for the invisible: Landscape change and ceramic manufacture during the Final Neolithic-Early Bronze Age at Phaistos (Crete, Greece). In: Ghilardi M (ed.) *La géoarchéologie des îles de Méditerranée* (Actes du colloque GEOMEDISLANDS, 30 juin–2 juillet 2015, Cargèse). Alpha: CNRS éditions, pp. 299–310.

Middleton GD (2010) *The Collapse of Palatial Society in LBA Greece and the Postpalatial Period* (BAR International Series 2110). Oxford: Archaeopress, p. 142.

Middleton GD (2017) *'The End of Minoan Crete*', *Understanding Collapse: Ancient History and Modern Myths*. Cambridge: Cambridge University Press, p. 462.

Monaco C and Tortorici L (2003) Effects of earthquakes on the Minoan 'royal villa' at Haghia Triada (Crete). *Creta Antiqua* 4: 403–417.

Monaco C and Tortorici L (2004) Faulting and effects of earthquakes on Minoan archaeological sites in Crete (Greece). *Tectonophysics* 382: 103–116.

Moody J (2000) Holocene climate change in Crete: An archaeologist's view. In: Halstead P and Frederick C (eds) *Landscape and Land Use in Postglacial Greece* (Sheffield Studies in Aegean Archaeology 3). Sheffield: Sheffield Academic Press, pp. 52–61.

Moody J, Rackham O and Rapp G (1996) Environmental archaeology of prehistoric NW Crete. *Journal of Field Archaeology* 23: 273–297.

Mourtzas ND and Marinos PG (1994) Upper Holocene sea-level changes: Paleogeographic evolution and its impact on coastal archaeological sites and monuments. *Environmental Geology* 23: 1–13.

Müller Celka S, Puglisi D and Bendali F (2014) Settlement pattern dynamics and resource exploitation in MM-LM I Crete: The case of Malia. In: Laffineur R, Procopiou H, Rougemont F et al. (eds) *PHYSIS. Natural Environment and Human Interaction in the Prehistoric Aegean* (Proceedings of the conference held in Paris (INHA), 11–14 December 2012, Aegaeum 37). Liège: Peeters, pp. 431–440.

Nakagawa T, Brugiapaglia E, Digerfeldt G et al. (1998) Dense-media separation as a more efficient pollen extraction method for use with organic sediment/deposit samples: Comparison with the conventional method. *Boreas* 27: 15–24.

Papadaki ES (2014) Monitoring subsidence at Messara basin using radar interferometry. *Environmental Earth Sciences* 72: 1965–1977.

Peterek A and Schwarze J (2002) Ruheloses Kreta. Hebungsgeschichte und Seismizität im Quartär und heute. *Geographische Rundschau* 54(4): 4–10.

Peterek A and Schwarze J (2004) Architecture and Late Pliocene to recent evolution of outer-arc basins of the Hellenic Subduction Zone (south-central Crete, Greece). *Journal of Geodynamics* 38(1): 19–55.

Psomiadis D, Dotsika E, Albanakis K et al. (2018) Speleothem record of climatic changes in the northern Aegean region (Greece) from the Bronze Age to the collapse of the Roman Empire. *Palaeogeography, Palaeoclimatology, Palaeoecology* 489: 272–283.

Quesnel Y, Jrad A, Mocci F et al. (2011) Geophysical signatures of a Roman and Early Medieval Necropolis. *Archaeological Prospection* 18: 105–115.

Rackham O and Moody J (1996) *The Making of the Cretan Landscape*. Manchester: Manchester University Press.

Rasmussen KL (2001) Provenance of ceramics revealed by magnetic susceptibility and thermoluminescence. *Journal of Archaeological Science* 28: 451–456.

Reille M (1992) *Pollen et spores d'Europe et d'Afrique du Nord*. Marseille: Laboratoire de Botanique historique et de Palynologie, 543 pp.

Reille M (1995) *Pollen et spores d'Europe et d'Afrique du Nord* (supplément 1). Marseille: Laboratoire de Botanique historique et de Palynologie, 327 pp.

Reille M (1998) *Pollen et spores d'Europe et d'Afrique du Nord* (supplément 2). Marseille: Laboratoire de Botanique historique et de Palynologie, 530 pp.

Reimer PJ, Bard E, Bayliss A et al. (2013) IntCal13 and MARINE13 radiocarbon age calibration curves 0–50000 years cal. BP. *Radiocarbon* 55(4): 1869–1887.

Roberts N (1979) The location and Environment of Knossos. *Annual of British School at Athens* 74: 231–241.

Roberts N, Eastwood WJ, Kuzucuoglu C et al. (2011) Climatic, vegetation and cultural change in the eastern Mediterranean during the mid-Holocene environmental transition. *The Holocene* 21(1): 147–162.

Rocchetti L (1967–1968) Il deposito protogeometrico di Petrokefali presso Festos. *Annuario della Scuola Archeologica di Atene* 29–30: 18–209.

Rocchetti L (1969–1970) Depositi sub-micenei e protogeometrici nei dintorni di Festòs. *Annuario della Scuola Archeologica di Atene* 47–48: 41–70.

Roether W, Manca BB, Klein B et al. (1996) Recent changes in eastern Mediterranean deep waters. *Science* 271: 333–335.

Rohling EJ, Mayewski PA, Hayes A et al. (2002) Holocene atmosphere-ocean interactions: Records from Greenland and the Aegean Sea. *Climate Dynamics* 18: 587–593.

Rossi A (in press) Surface Field Survey and Remote Sensing at Phaistos: Preliminary Report 2008–2010. In: 11th International Cretological Congress, Rethymno, 21–27 October 2011.

Round FE, Crawford RM and Mann DG (1990) *The Diatoms, Biology & Morphology of the Genera*. Cambridge: Cambridge University Press.

Sandars NK (1978) *The Sea Peoples: Warriors of the Ancient Mediterranean, 1250-1150 B.C*. London: Thames & Hudson, p. 224.

Shaw JW and Shaw MC (1995) *Kommos: An Excavation on the South Coast of Crete*. Princeton, NJ: Princeton University Press, 818 pp.

Siart C, Hecht S, Holzhauer I et al. (2010) Karst depressions as geoarchaeological archives: The palaeoenvironmental reconstruction of Zominthos (Central Crete) based on geophysical prospection, mineralogical investigations and GIS. *Quaternary International* 216: 75–92.

Stuiver M and Reimer PJ (1993) Extended 14C data base and revised CALIB 3.0 14C age calibration program. *Radiocarbon* 35: 215–230.

Theocharis A, Nittis H, Kontoyiannis E et al. (1999) Climatic changes in the Aegean Sea influence the Eastern

Mediterranean thermohaline circulation (1986–1997). *Geophysical Research Letters* 26(11): 1617–1620.

Theodorakopoulou K and Bassiakos Y (2017) Geoarchaeological studies at the cemetery of ancient Kamara, assisted by optically stimulated luminescence (OSL) dating: Insights in the post-Roman hydrological record of Eastern Crete. *Journal of Archaeological Science: Reports* 12: 794–804.

Theodorakopoulou K, Pavlopoulos K, Athanassas K et al. (2012) Sedimentological response to Holocene climate events in the Istron area, Gulf of Mirabello, NE Crete. *Quaternary International* 266: 62–73.

Theodorakopoulou K, Pavlopoulos K, Triantaphyllou MV et al. (2009) Geoarchaeological studies in the coastal area of Istron-Kalo Chorio (Gulf of Mirabello-Eastern Crete): Landscape evolution and paleoenvironmental reconstruction. *Zeitshrift für Geomorphologie* 53(Suppl. 1): 55–70.

Todaro S (2013) *The Phaistos Hills Before the Palace: A Contextual Reappraisal* (Praehistorica Mediterranea 5). Monza: Polimetrica, International Scientific Service.

Todaro S and Di Tonto S (2008) The Neolithic settlement of Phaistos revisited: Evidence for ceremonial activity on the eve of Bronze Age (ed V Isaakidou and P Tomkins; *Escaping the Labirinth: The Cretan Neolitic in Contex, Sheffield Studies*). *Aegean Archaeology* 8: 177–190.

Tsapanos TM (2001) Earthquake hazard parameters estimated in Crete Island and the adjacent area. *Pure Applied Geophysics* 158: 1691–1718.

Tsonis AA, Swanson KL, Sugihara G et al. (2010) Climate change and the demise of Minoan civilization. *Climate of the Past* 6: 525–530.

Turland NJ, Chilton L and Press JR (1993) Flora of the Cretan area. London: HMSO, 439 pp.

Vokotopoulos L, Plath G and McCoy FW (2014) The yield of the land: Soil conservation and the exploitation of arable land at choiromandres, zakros in the new palace period. In: Laffineur R, Procopiou H, Rougemont F et al. (eds) *PHYSIS. Natural Environment and Human Interaction in the Prehistoric Aegean (Proceedings of the conference held in Paris (INHA)*, 11–14 December 2012, Aegaeum 37). Liège: Peeters, pp. 251–262.

Watrous LV, Hadzi-Vallianou D and Blitzer H (2004). *The Plain of Phaistos* (Monographs 23). Los Angeles, CA: Cotsen Institute of Archaeology, UCLA.

Watrous LV, Xatzi-Vallianou D, Pope K et al. (1993) A survey of the western Mesara plain in Crete: Preliminary report of the 1984, 1986, and 1987 field seasons. *Hesperia: The Journal of the American School of Classical Studies at Athens* 62(2): 191–248.

Weiberg E, Unkel I, Kouli K et al. (2016) The socio-environmental history of the Peloponnese during the Holocene: Towards an integrated understanding of the past. *Quaternary Science Reviews* 136: 40–65.

Weiss B (1982) The decline of Late Bronze Age civilization as a possible response to climatic change. *Climatic Change* 4(2): 173–198.

Weiss H (2016) Global megadrought, societal collapse and resilience at 4.2-3.9 ka BP across the Mediterranean and the west Asia. *PAGES Magazine* 24(2): 62–63.

Xoplaki E (2002) *Climate variability over the Mediterranean*. PhD Thesis, University of Bern, p. 193.

Zanchetta G, Regattieri E, Isola I et al. (2016) The so-called '4.2 event' in the central Mediterranean and its climatic teleconnections. *Alpine and Mediterranean Quaternary* 29(1): 5–17.

Zervakis V, Georgopoulos D and Drakopoulos PG (2000) The role of the North Aegean in triggering the recent Eastern Mediterranean climatic changes. *Journal of Geophysical Research* 105: 26103–26116.

Zervakis V, Georgopoulos D, Karageorgis AP et al. (2004) On the response of the Aegean Sea to climatic variability: A review. *International Journal of Climatology* 24: 1845–1858.

Zielhofer C, Faust D and Listädter J (2008) Late Pleistocene and Holocene alluvial archives in the southwestern Mediterranean: Changes in fluvial dynamics and past human response. *Quaternary International* 181: 39–54.